Rheology of highly concentrated planar fiber suspensions

Steven Le Corre[a)]

GeM-Institut de Recherche en Génie Civil et Mécanique, CNRS-Ecole Centrale de Nantes, BP 92101, 44321 Nantes Cedex 3, France

Pierre Dumont[b)]

Laboratoire de Technologie des Composites et Polymères, Institut des Matériaux, Ecole Polytechnique Fédérale de Lausanne, MX-G 136 Station 12, CH-1015 Lausanne, Switzerland

Laurent Orgéas[c)] and Denis Favier[d)]

Laboratoire Sols-Solides-Structures (3S), CNRS-Universités de Grenoble (INPG-UJF), BP 53, 38041 Grenoble Cedex 9, France

(Received 7 January 2005; final revision received 27 May 2005)

Synopsis

The rheology of highly concentrated fibers suspended in power-law fluids is investigated by upscaling the physics at the fiber scale. A deterministic upscaling technique is used, namely the homogenization method for periodic discrete structures. This micro-macro approach is used to carry out a quantitative study of concentrated fiber suspensions with planar fiber orientation, performing "numerical rheometry experiments" on a set of representative elementary volumes of fiber suspensions. The simulations underline the significant influence of the fiber volume fraction and orientation, as well as of the non-Newtonian properties of the suspending fluid on the resulting macroscopic rheological behavior. The predictions of the model are compared with experimental results obtained on an industrial thermoset short fiber-bundle polymer composite (SMC). © *2005 The Society of Rheology.* [DOI: 10.1122/1.1993594]

I. INTRODUCTION

Due to their interesting mechanical and thermo-physical specific properties and their cost efficient processing, fiber reinforced polymer composites are attractive materials in many applications (Advani, 1994; Berglund and Ericson, 1995). For example, sheet molding compounds (SMC) or glass mat thermoplastics (GMT) are now widely used in the automotive or electrical industries to produce semi-structural and lightweight parts. These composites have quite similar characteristics: they are 1 to 4-mm-thick pre-impregnated sheets in which "short" glass fibers or glass fiber bundles (length

[a)]Author to whom correspondence should be addressed; electronic mail: steven.le-corre@ec-nantes.fr
[b)]Electronic mail: pierre.dumont@epfl.ch
[c)]Electronic mail: laurent.orgeas@hmg.inpg.fr
[d)]Electronic mail: denis.favier@hmg.inpg.fr

≈5–50 mm, weight fraction 10%–30%) have an initial random planar orientation and constitute the reinforcement. The matrix is a filled thermoset resin in the case of SMC, whereas it is a thermoplastic polymer for GMT. SMC are processed by compression molding: stacked charges made of 1–10 cold (≈296 K) sheets are rapidly squeezed (mold closure speed ≈0.1-10 mm s^{-1}) in a hot mold (≈423 K). The compression molding or stamping of GMT is very similar, except the temperature of the initial charges (≈423 K) and the temperature of mold (≈296 K). This flowing stage is followed by a period of ≈30 s to 5 min, during which the polymer matrix cures (SMC) or cools down (GMT), before ejecting the produced part from the mold. During the flowing stage, short fiber composites can be seen as very concentrated fiber suspensions, whose suspending fluid displays a non-Newtonian behavior. Understanding and modeling the strong coupling between the mechanical behavior of these suspensions and their microstructure is a key problem towards a good description of the rheology of such materials and the optimization of composites manufacturing. For example, it is well known that the fiber content and the evolution of fiber orientation during the forming process strongly affects the final geometry and the properties of the produced parts (Osswald and Tseng, 1994; Thomasson and Vlug, 1996).

Fiber suspensions have a rather complex rheological behavior governed by microstructural parameters such as the fiber concentration, orientation and spatial distribution, the mechanical properties of the fibers and the matrix, and the matrix-fiber or fiber-fiber interaction mechanisms. The deformation mode of the suspension depends on its concentration regime. Within the *dilute regime*, it is assumed that the perturbation of the flow field in the matrix near a fiber is not affected by the presence of the others because the fibers are sufficiently far apart from each other. Within the *semidilute regime*, fibers have hydrodynamic interactions because the flow field perturbations surrounding the fibers overlap. Within the *concentrated regime*, the average distance between the fibers is of the order of fiber diameter so that fibers interact through hydrodynamic and also direct contact effects. Fiber composites such as GMT and SMC belong to this category: their high fiber content and their "planar" fiber orientation are such that fibers or fiber bundles are strongly entangled, bend, and experience multiple contacts with their neighbors.

The modelling of dilute and semidilute suspensions has been addressed in a lot of theoretical and numerical studies. Theories are now well-established for suspensions of rigid fibers in Newtonian solvents. Most models are based on the fundamental pioneering works of Jeffery and Batchelor. Jeffery (1922) analyzed the motion of a rigid small ellipsoidal particle in an infinite incompressible Newtonian solvent, with no external forces or torques or Brownian motion, and determined the stress state near the particle. This approach gave rise to different models of suspensions of ellipsoids in the dilute or semidilute regimes (Ausias *et al.*, 1992; Lipscomb *et al.*, 1988; Phan-Thien and Graham, 1991). Batchelor has a predominant influence on fiber suspensions modeling theories. First he gave a general framework for mechanical models for suspensions (Batchelor, 1970a, 1974), second he developed slender body theories to determine the force applied on a particle and particle flow interaction (Batchelor, 1970b), third he modeled the behavior of semidilute suspensions of aligned fibers (Batchelor, 1971). A generalization of the last problem to arbitrary orientation distribution was achieved by Dinh and Armstrong (1984). The semidilute theory was further developed by Shaqfeh, Koch, Fredrickson, and co-workers (Koch, 1995; Koch and Shaqfeh, 1990; Shaqfeh and Koch, 1990) and validated by means of experiments (Petrich *et al.*, 2000) or numerical simulation (Mackaplow and Shaqfeh, 1996; Sundararajakumar and Koch, 1997). Notice that all these models lead to a common expression for the macroscopic stress tensor of the suspension $\boldsymbol{\sigma}^s$:

$$\boldsymbol{\sigma}^{(s)} = -p^{(s)}\boldsymbol{\delta} + \boldsymbol{\sigma}^{(m)} + \boldsymbol{\sigma}^{(f)}, \tag{1}$$

where the pressure $p^{(s)}$ is related to the assumed incompressibility of the suspension, and where $\boldsymbol{\sigma}^{(m)}$ and $\boldsymbol{\sigma}^{(f)}$ are bulk extra stress contributions due to the matrix and fibers, respectively. $\boldsymbol{\sigma}^{(f)}$ depends on matrix-fiber but also fiber-fiber interactions. Also notice that these models account for fiber orientation; this is usually done using the orientation tensors [see for instance the review by Dupret and Verleye (1999)], which are compact, efficient macroscopic measurement of fiber orientation. The influence of fiber orientation on the overall behavior of the suspensions is accounted for by coupling anisotropic constitutive expressions of $\boldsymbol{\sigma}^{(s)}$ with a set of equations modeling the change of the orientation tensors during the flow (Ausias *et al.*, 1992; Dupret and Verleye, 1999; Hand, 1962; Hinch and Leal, 1975; Munganga *et al.*, 2000). This system of equations is often based on an extension of the fundamental problem of the orientation evolution of a slender particle suspended in a infinite incompressible Newtonian fluid for the dilute or semidilute regimes of concentration (Bretherton, 1962; Fan *et al.*, 1998; Folgar *et al.*, 1984; Jeffery, 1922; Koch, 1995, Phan-Thien *et al.*, 2002; Rahnama *et al.*, 1995). Closure approximations of the fourth-order orientation tensor in terms of the second-order orientation tensor were developed to simplify calculations (Advani and Tucker, 1987, 1990; Chung and Kwon, 2002; Cintra and Tucker III, 1995; Dupret and Verleye, 1999; Hand, 1962; Hinch and Leal, 1976). The problem of closure approximations has attracted a lot of attention during the past decades. It remains a difficult one: for example, it has been shown that some closure approximations could provide kinematic or thermodynamic anomalies (Galdi and Reddy, 1999; Munganga *et al.*, 2000), whereas others are more or less relevant depending on the local flow and the current orientation of fibers. At last, all the approaches cited above are devoted to Newtonian suspending fluids. To our knowledge, few contributions analyze and model the mechanical behavior of fiber suspensions in power-law fluids (Gibson and Toll, 1999; Goddard, 1976; Souloumiac and Vincent, 1998), which are of interest in compounds such as SMC or GMT. In a sense, these studies are extensions of the works of Batchelor (1971) and Dinh and Armstrong (1984).

In order to describe the rheology of concentrated fiber suspensions, semidilute models have been applied although the description of local mechanisms of interactions between fibers remains unappropriate for such materials. Indeed, Mackaplow and Shaqfeh (1996) showed that the comparison of the predicted viscosities of theories and simulations based on hydrodynamic fiber-fiber interactions with experimental measurements reveals divergence in the concentrated regime. Such a deviation was explained by the leading role of mechanical contacts between fibers in the concentrated regime, this type of fiber-fiber interaction being omitted in semidilute theories. The nature of fiber-fiber contact in the concentrated regime was further investigated experimentally with Newtonian fiber suspensions (Petrich and Koch, 1998) and non-Newtonian fiber or fiber bundle suspensions (Ericsson *et al.*, 1997; Servais *et al.*, 1999a, b). Conclusions drawn from these works tend to prove that fiber-fiber contact efforts are ruled by Coulombic friction and lubrication mechanisms, the last one being linked to the deformation of a thin amount of entrapped matrix (e) in the contact zones. Following such experimental evidence, several numerical studies using particle-level simulation methods have been carried out to understand the behavior of concentrated suspensions and model their macroscopic rheology (Fan *et al.*, 1998; Joung *et al.*, 2001, 2002; Sundararajakumar and Koch, 1997; Switzer and Klingenberg, 2003; Yamane *et al.*, 1995). Considered fibers are straight and rigid (Fan *et al.*, 1998; Sundararajakumar and Koch, 1997; Yamane *et al.*, 1995), or flexible and curved (Joung *et al.*, 2001, 2002; Switzer and Klingenberg, 2003), and have three-dimensional orientation. Mechanical contacts between fibers induce frictionless non-hydrodynamic

(Sundararajakumar and Koch, 1997), lubrication (Fan *et al.*, 1998; Joung *et al.*, 2001, 2002, Yamane *et al.*, 1995) or Coulombic contact forces (Switzer and Klingenberg, 2003), arising from the relative motion of connected fibers. Notice that in all these sophisticated numerical studies, (i) the considered suspending fluid is restricted to the Newtonian case, (ii) none of them use non-Newtonian viscous contact forces, and (iii) no contact moments are considered. In parallel, Toll and Månson (1994) have proposed a probabilistic model well suited for concentrated suspensions with non-Newtonian suspending fluid and planar fiber orientation. In this model, more realistic mechanisms for interaction forces were considered: at each contact point between two fibers, the force exerted by one on the other is composed of a normal and a tangential component. The normal one is purely elastic and reflects the elastic bending of fiber in the thickness of the planar suspension: it is a power-law function of the fiber volume fraction, with a power-law exponent of 5. The tangential one is a friction force that depends on the sliding velocity at the contact point and on the normal force. Servais *et al.* have specified more precisely this tangential component for fiber suspensions (Servais *et al.*, 1999b) or bundle ones (Servais *et al.*, 1999a), splitting it into two contributions: a dry or Coulombic friction contribution, function of the normal component and the sliding velocity direction, and a lubrication contribution, induced by the shearing of a small amount of entrapped fluid (e) at the interface between two contacting or almost contacting fibers or bundles. The lubrication contribution is a power-law (Servais *et al.*, 1999b) or a Carreau type (Servais *et al.*, 1999a) function of the sliding velocity, which power-law exponent (or strain-rate sensitivity index) is the same as that of the suspending fluid. It is also a square function of the fiber volume fraction. However, as in the particle level simulation models, contact moments have been neglected in their micromechanical analysis. Moreover, rather strong kinematical assumptions were postulated for the in-plane motion of fibers: the velocity of the center of each fiber was assumed to be that of the bulk suspension and the rotation of a fiber was supposed to be an affine function of the macroscopic velocity gradient.

Within that context, a theoretical investigation based on a deterministic upscaling technique has been recently proposed to establish the fundamental properties of the macroscopic mechanical behavior of networks of fibers, looked as bars, linked by power-law viscous joints that induce forces but also moments during the relative motion of contacting fibers (Le Corre *et al.*, 2004). Such microstructures and mechanical fiber-fiber interactions are rather close to those encountered in highly concentrated suspensions with power-law suspending fluid such as GMT or SMC. Unfortunately, in this purely theoretical work, no quantitative study was developed in order to link constitutive parameters of the macroscopic mechanical behavior with microstructural ones. Hence, the aim of the present contribution is first to study quantitatively the deformation of concentrated non-Newtonian fiber bundle suspensions displaying a planar bundle orientation pursuing the theoretical framework proposed in Le Corre *et al.*, (2004) and adopting bundle-bundle contact mechanisms close to that encountered in industrial planar short fiber composites, i.e., similar to those proposed by Toll and co-workers (Ericsson *et al.*, 1997; Servais *et al.*, 1999a, b; Toll and Månson, 1994). The other point is then to emphasize the role of the microstructure on the resulting macroscopic mechanical behavior and compare the prediction of the established micro-macro model with experimental results obtained from an industrial SMC (Dumont *et al.*, 2003; Le Corre *et al.*, 2002). For that purpose, the basic assumptions of the model derived by Le Corre *et al.* (2004) as well as the micromechanical analysis of the motion of bundles and interactions are given in Sec. II. A brief presentation of both the upscaling technique and the fundamental results deduced from it are given in Sec. III. In Sec. IV, we introduce the numerical scheme that was developed

to study quantitatively the macroscopic mechanical behavior of typical planar concentrated bundle suspensions. This finally enables one to compare numerical simulation results with rheometry experiments performed with an industrial SMC (Sec. V) and to discuss some of the hypotheses made in the micromechanical analysis (Sec. VI).

II. PROBLEM STATEMENT AND IDEALIZATION

A. Notation

For the rest of the document, please notice that in order to distinguish phenomena arising at the microscopic scale inside the polymer matrix (m), the fibers (f), or in the whole suspension (s), from those "apparently" resulting at the macroscopic scale, we introduce a specific notation for microscopic and macroscopic quantities: if ϕ is a scalar physical quantity, then $\phi_{(\alpha)}$ (with the subscript $_{(\alpha)}$) is the microscopic or local value of ϕ in phase α (s,m, or f), whereas $\phi^{(\alpha)}$ (with the exponent $^{(\alpha)}$) is the macroscopic or averaged value of ϕ for the same constituent.

B. Basic assumptions

The suspensions under consideration in the present contribution are SMC or GMT-like materials: they are sheets of thickness h in which fiber bundles of length l are homogeneously distributed in the plane of the sheets $\mathcal{P}\equiv(\boldsymbol{e}_1,\boldsymbol{e}_2)$ and immersed in a non-Newtonian fluid. The thickness of the sheet ($\boldsymbol{e}_3$ direction) is supposed to be small compared to the length of the fiber bundles ($h \ll l$). Moreover, the fiber suspensions are sufficiently concentrated to form networks of contacting bundles. At the microscopic or local scale, i.e., at the bundle scale, the deformation of the suspension is therefore mainly ruled by bundle-bundle short range interactions. Such an assumption is supported by experimental results obtained on industrial SMC or GMT (Dumont *et al.*, 2003; Ericsson *et al.*, 1997; Le Corre *et al.*, 2002; Servais *et al.*, 1999a, 2002, 1999b). At the macroscopic scale, this leads to neglect $\boldsymbol{\sigma}^{(m)}$ in Eq. (1):

$$\boldsymbol{\sigma}^{(s)} \approx -p^{(s)}\boldsymbol{\delta} + \boldsymbol{\sigma}^{(f)}. \tag{2}$$

In addition, the suspension is assumed perfectly saturated and the matrix as well as the bundle incompressible, so that the suspension is considered as incompressible. At last, inertia effects will be neglected. Such an assumption is supported both by the rheological properties of SMC or GMT materials (density $\approx$2000 kg m^{-3}, viscosity ranging from 10^3 to 10^9 Pa s) and by the typical processing parameters that involve in-plane velocities ranging from 10^{-2} to 1 m s^{-1} and thicknesses of 1 to 10 mm. The resulting Reynolds number R_e rarely exceeds 10^{-2}.

To evaluate the macroscopic fiber stress tensor $\boldsymbol{\sigma}^{(f)}$ under such circumstances, a deterministic upscaling technique is used (see Sec. III). As in all homogenization processes, it is of great importance to emphasize that the heterogeneous local deformation of the described suspensions can be homogenized, i.e., can be modeled by an equivalent continuous macroscopic description, provided that the condition of scale separation is satisfied. For the suspensions under consideration, this fundamental condition may be expressed as

$$\epsilon = \frac{d}{L} \ll 1, \tag{3}$$

where d and L are, respectively, the characteristic lengths of the heterogeneities at the bundle scale and of the macroscopic sample, as illustrated in Fig. 1. In industrial SMC or

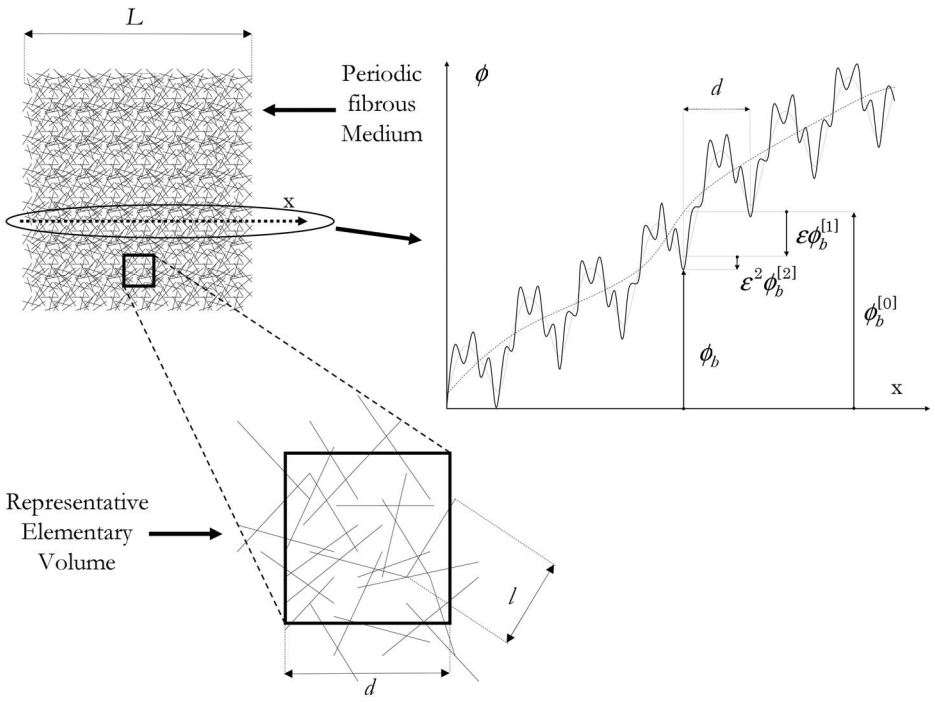

FIG. 1. Homogenization method for discrete and periodic media: basic principle and specific asymptotic expansions.

GMT, d is of the order of the fiber length l ($\approx$25 mm), whereas L can be considered as the typical size of industrial molded parts ($\approx$1 m): this leads to a rather good scale separation about 2.5×10^{-2}.

C. Micromechanical analysis

1. Bundles geometry

Figure 2 gives an optical micrography showing cross sections of typical industrial glass fiber bundles used in SMC. These bundles are made of about 200 fibers of diameter 15 μm, and have a rather flat cross section, with an average major dimension $d^0_{\max}$ of

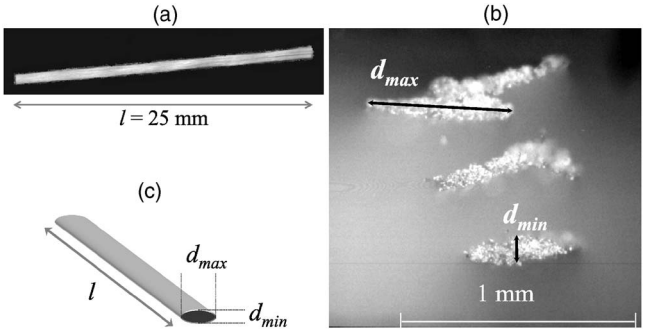

FIG. 2. Optical micrographies showing typical glass fiber-bundles used in industrial SMC: (a) top view of bundles, (b) cross-sections of bundles, (c) idealization of bundles geometry.

0.6 mm±15% and an average minor dimension $d^0_{\min}$ of 0.06 mm±15%. In the following, we will assume that the bundles have homogeneous constant elliptical cross sections, which major and minor axes are $d^0_{\max}$ and $d^0_{\min}$, respectively.

Before being introduced in the compounds, bundles are straight cylinders of length l (for the bundles displayed in Fig. 2, $l=25$ mm). Note that the aspect ratios $d^0_{\max}/l$ and $d^0_{\min}/d^0_{\max}$ of the considered fiber bundles are of the order of the scale separation parameter ϵ, i.e., $d^0_{\max}/l=\mathcal{O}(\epsilon)$ and $d^0_{\min}/d^0_{\max}=\mathcal{O}(\epsilon)$. When the bundles are introduced in the industrial sheet compounds, they are submitted to a packing stress perpendicular to the plane of the sheet. This initial packing stage is such that the volume fraction of bundles in the sheet is largely higher than the maximum volume fraction that can be reached with strictly rigid and straight bundles. This implies the following:

(1) Bundles flatten normal to the packing stress, so that the major axis $d_{\max} \geqslant d^0_{\max}[=\mathcal{O}(d^0_{\max})]$, is perpendicular to the packing stress. Conversely the minor axis $d_{\min} \leqslant d^0_{\min}[=\mathcal{O}(d^0_{\min})]$ is parallel to the packing stress.
(2) Bundles are bent mainly around the major axis $d_{\max}$, thus in the thickness of the sheet. As the thickness of the sheets $h \approx 2$–3 mm is rather small compared to the length l of bundles, i.e., $h/l=\mathcal{O}(\epsilon)$, we will consider that each bundle b has a mean orientation along a unit vector $\boldsymbol{e}_b$ contained in the plane $\mathcal{P}$.

2. Bundles kinematics

To study the rheology of the bundle suspensions under consideration, several kinematical restrictions are stated. They are listed in the following points.

(1) As first approximations, similar to that proposed by Servais *et al.* (1999a), the bending of bundles in $\mathcal{P}$ is neglected and the bundles are assumed to keep a constant elliptical cross section during the deformation. Let us consider point K located at a curvilinear abscissa s_b and an altitude z_b from the center of mass G_b of bundle b ($\boldsymbol{G_bK}=s_b\boldsymbol{e}_b+z_b\boldsymbol{e}_3$). Introducing $\tilde{\boldsymbol{u}}$ as the projection of $\boldsymbol{u}$ in $\mathcal{P}$, the velocity $\tilde{\boldsymbol{v}}_b(K)$ of K may therefore be written as

$$\tilde{\boldsymbol{v}}_b(K)=\tilde{\boldsymbol{v}}_b+s_b\omega_b\boldsymbol{e}_3\times\boldsymbol{e}_b, \tag{4}$$

where $\tilde{\boldsymbol{v}}_b$ and ω_b are, respectively, the in-plane velocity of G_b and the angular velocity of the bundle about $\boldsymbol{e}_3$. This can also be written as

$$\tilde{\boldsymbol{v}}_b(K)=\tilde{\boldsymbol{v}}_b+\epsilon\, s^*_b\phi_b\boldsymbol{e}_3\times\boldsymbol{e}_b, \tag{5}$$

where $s^*_b=s_b/d$ is the local abscissa of K on bundle b normalized with respect to d, and where $\phi_b=L\omega_b$ is introduced in order to normalize angular velocities with respect to linear velocities (Le Corre *et al.*, 2004).

(2) Because of the very high bundle content, the low ratios $d_{\min}/d_{\max}$ and h/l, the rotation of the bundles about axis contained in $\mathcal{P}$ is considered as negligible, so that during the deformation, the major dimensions l and $d_{\max}$ stay in $\mathcal{P}$. If $\boldsymbol{\omega}_b(K)$ is the local angular velocity of the bundle, this yields

$$\boldsymbol{\omega}_b\approx\omega_b\boldsymbol{e}_3. \tag{6}$$

One can finally write:

$$\boldsymbol{v}_b(K)=\tilde{\boldsymbol{v}}_b+\epsilon\, s^*_b\phi_b\boldsymbol{e}_3\times\boldsymbol{e}_b+v_{3b}\boldsymbol{e}_3, \tag{7}$$

where v_{3b} is due on one hand to the overall motion of the suspension along $\boldsymbol{e}_3$ and on the other hand to the bending of the bundles about axis contained in $\mathcal{P}$.

(3) The macroscopic shearing in the thickness of the sheets will not be investigated in the present contribution: noting $\boldsymbol{L}^{(s)}=\mathrm{grad}(\boldsymbol{v}^{(s)})$ the macroscopic velocity gradient of the suspension, only situations for which $L_{i3}=L_{3i}=0$ $(i=1,2)$ will be explored.

To summarize, these assumptions lead to restrict the present model (i) to thin concentrated suspensions where fiber bundles have and keep a mean planar orientation and display small deformation during the flow, (ii) to situations where no out of plane shearing occurs. Notice that these assumptions are not a restriction of the proposed methodology which could be extended to thick three-dimensional suspensions containing straight or curved flexible fibers, and to any given macroscopic velocity gradient.

3. Bundle-bundle mechanical interaction

As mentioned in Sec. I, the complex bundle-bundle interactions occurring during the deformation of concentrated suspensions have been modeled by means of normal forces and tangential lubrication and/or Coulombic friction forces (Ericsson *et al.*, 1997; Servais *et al.*, 1999a, b). Rheometry experiments performed on highly concentrated suspensions made of fibers or bundles of fibers give useful information about the predominant type of interaction (Dumont *et al.*, 2003; Ericsson *et al.*, 1997; Le Corre *et al.*, 2002; Servais *et al.*, 1999a, 2002, 1999b). When the fiber content is "high," the macroscopic strain rate is "low," and the viscosity of the matrix is "low," then the elastic normal forces as well as dry friction tangential forces seem to play a key role on the overall behavior of the suspension. Conversely, tangential lubrication forces seem to govern the rheology at "lower" fiber contents, "higher" macroscopic strain rates, and "high" matrix viscosity. More precisely, bundle suspensions such as SMC and GMT that are deformed within macroscopic strain rates and bundles content ranges encountered during their processing (respectively, from 10^{-2} to 10^{2} s^{-1}, and from 5wt % to 30wt %) behave as a first and reasonable approximation as purely viscous anisotropic fluids whose macroscopic viscosities are (i) power-law or Carreau-type functions of the macroscopic strain rate state (Dumont *et al.*, 2003; Servais *et al.*, 1999a, 2002) and (ii) quadratic functions of the bundle content (Dumont *et al.*, 2003).

Within the concepts proposed by Toll and Månson (1994), and accounting for the above experimental evidence, the following assumptions will be further done for the bundle-bundle interactions:

(1) interaction forces normal to plane $\mathcal{P}$, that are mainly induced by the in-thickness elastic bending of the bundles will be considered as negligible:

$$\boldsymbol{f}_k \cdot \boldsymbol{e}_3 \cong 0 \Leftrightarrow \boldsymbol{f}_k \cong \widetilde{\boldsymbol{f}}_k, \tag{8}$$

(2) possible associated Coulombic friction forces will therefore be neglected,
(3) the bundle-bundle interactions are due to lubrication forces but also lubrication moments, both induced by the shearing of a small amount of an incompressible and purely viscous medium (e) entrapped between bundles in contact.

The geometry of the viscous medium (e) (the contact zone), its microstructure and its rheology may be very complex. Only *in situ* observations of contact zones during the deformation of the bundle suspension would allow one to determine their global geometry, the microstructure (homogeneous/heterogeneous), and the deformation micromechanisms of the entrapped viscous medium in order to build a pertinent micromechanical model. For the moment, using the fact that $d_{\max}$ is about ten times greater than $d_{\min}$, we simply assume that this complex situation is equivalent to the shearing of a thin prism of

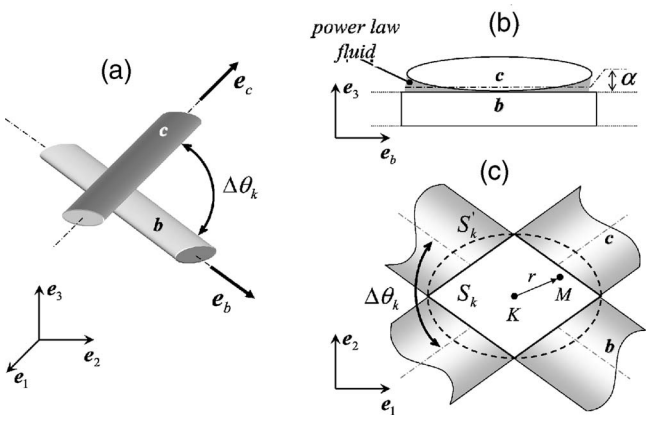

FIG. 3. Modeling of bundle-bundle local interactions: side view of the interaction zone (b), top view of the interaction surface approximation for local moments evaluation (c).

height α (see Fig. 3) of an equivalent homogeneous entrapped viscous fluid (e), which rheology is given by the following power-law model:

$$\boldsymbol{\sigma}_{(e)} = -p_{(e)}\boldsymbol{\delta} + 2\eta_{(e)}\left(\frac{\dot{\gamma}_{(e)}}{\dot{\gamma}_0}\right)^{(m-1)}\boldsymbol{D}_{(e)}, \tag{9}$$

where $\boldsymbol{\sigma}_{(e)}$ and $p_{(e)}$ are, respectively, the local stress tensor and pressure in the equivalent entrapped fluid, $\dot{\gamma}_{(e)}$ the local shear rate, $\eta_{(e)}$ is the viscosity of the fluid at a characteristic shear rate $\dot{\gamma}_0$ arbitrarily fixed to 1 s^{-1}, $\boldsymbol{D}_{(e)}$ the local strain rate tensor, and m the power-law exponent.

In the case of an ideal power-law matrix, $\eta_{(e)}$ and m would be exactly the same as the viscosity and the power-law exponent of the bulk matrix. For a polymer matrix (GMT), it is well known that the power-law model is a first approximation of the polymer viscosity that is only acceptable within a restricted shear rate range: the viscosity $\eta_{(e)}$ and the power-law exponent m of the entrapped fluid should correspond to those which should be measured on the bulk polymer matrix tested under the same shear rates. For pasty matrices (e.g., SMC, see Sec. V), which include a great amount of mineral charges with a mean diameter of the same order of magnitude as the diameter of the fibers contained in a bundle, no such straightforward correlation can be done. $\eta_{(e)}$ and m can for example be determined from "bundle pull-out experiments" similar to those performed by Servais *et al.* (1999a), or directly using a rheometry experiment on the whole bundle suspension (see Sec. V B).

Thereby, it was finally assumed that during the relative displacement of a couple k of connected bundles b and c (the center of the contact zone is noted K), the entrapped fluid is submitted to the superposition of:

(1) a uniform planar simple shear at the shear rate $\dot{\gamma}_{1(e)}$, due to the in plane difference of velocities of bundles $\Delta\tilde{\boldsymbol{v}}_k$:

$$\dot{\gamma}_{1(e)} = \frac{\|\tilde{\boldsymbol{v}}_b(K) - \tilde{\boldsymbol{v}}_c(K)\|}{\alpha} = \frac{\|\Delta\tilde{\boldsymbol{v}}_k\|}{\alpha}, \tag{10}$$

(2) a rotating planar shear $\dot{\gamma}_{2(e)}(r)$ due to the difference of angular velocities of bundles $\Delta\boldsymbol{\omega}_k=\Delta\omega_k\boldsymbol{e}_3$, where $r=\|\boldsymbol{KM}\|$ is the distance of the considered point M to the center of the contact zone K [see Fig. 3(c)]. This shear rate is

$$\dot{\gamma}_{2(e)}(r)=r\frac{\|\boldsymbol{\omega}_b-\boldsymbol{\omega}_c\|}{\alpha}=r\frac{\|\Delta\omega_k\|}{\alpha}. \tag{11}$$

In order to evaluate the expressions and the order of magnitude of both interaction forces and moments, two separate situations are considered. The interaction force $\boldsymbol{f}_k$ exerted by the bundle c on the bundle b is evaluated by considering the case where $\Delta\boldsymbol{\omega}_k=\boldsymbol{0}$, whereas the interaction moment $\boldsymbol{M}_k(K)=M_k(K)\boldsymbol{e}_3$ is evaluated in the case $\Delta\boldsymbol{v}_k=\boldsymbol{0}$. A real planar motion however generally implies both effects but those two limiting cases should give a good approximation. According to Eq. (9), the norm of $\boldsymbol{f}_k$ is defined as

$$\|\boldsymbol{f}_k\|=\int_{S_k}\eta_{(e)}\left(\frac{\dot{\gamma}_{1(e)}}{\dot{\gamma}_0}\right)^{m-1}\dot{\gamma}_{1(e)}dS, \tag{12}$$

where S_k denotes the surface of the connection k in the plane of bundles, characterized by $d_{\max}$ and $\Delta\theta_k$, the relative angle between both connected bundles (see Fig. 3). The shear rate being assumed homogeneous, a rather simple expression of $\boldsymbol{f}_k$ can therefore be established:

$$\boldsymbol{f}_k=\frac{\eta_{(e)}}{\alpha}\frac{d_{\max}^2}{|\sin\Delta\theta_k|}\left(\frac{\|\Delta\tilde{\boldsymbol{v}}_k\|}{\alpha\dot{\gamma}_0}\right)^{m-1}\quad\Delta\tilde{\boldsymbol{v}}_k=\mu_k\|\Delta\tilde{\boldsymbol{v}}_k\|^{m-1}\Delta\tilde{\boldsymbol{v}}_k. \tag{13}$$

In the same way, moments intensities $|M_k(K)|$ are defined as

$$|M_k(K)|=\int_{S_k}\eta_{(e)}\left(\frac{\dot{\gamma}_{2(e)}}{\dot{\gamma}_0}\right)^{m-1}\dot{\gamma}_{2(e)}rdS. \tag{14}$$

No such simple result can be drawn in that case. Nevertheless, an upper bound $|M'_k(K)|$ of $|M_k(K)|$ can be found, using the elliptical surface S'_k instead of S_k [see Fig. 3(c)]. The integration of Eq. (14) on S'_k provides the following result:

$$|M_k(K)|<|M'_k(K)|,$$

$$M'_k(K)=\mu_k\left[\frac{\pi}{m+3}\left(\frac{d_{\max}}{|\sin\Delta\theta_k|}\right)^{m+1}\right]|\Delta\omega_k|^{m-1}\Delta\omega_k. \tag{15}$$

Using $\phi_b=\omega_b/L$ and introducing $m_k=M'_k(K)/L$, this last expression can also be written as

$$m_k=\mu_k\left[\frac{\pi}{(m+3)|\sin\Delta\theta_k|^{m+1}}\left(\frac{d_{\max}}{L}\right)^{m+1}\right]|\Delta\phi_k|^{m-1}\Delta\phi_k$$

$$=\beta_k|\Delta\phi_k|^{m-1}\Delta\phi_k, \tag{16}$$

where coefficient β_k has the same unit as the viscosity μ_k.

4. Momentum balance for a bundle

Neglecting acceleration and external volume forces and moments, and introducing $\mathcal{C}_b$ the set of connections of bundle b, the momentum balance of a given bundle b can be written as

$$\forall b, \quad \begin{cases} \displaystyle\sum_{k\in\mathcal{C}_b} \boldsymbol{f}_k = \boldsymbol{0} & \text{(17a)} \\ \displaystyle\sum_{k\in\mathcal{C}_b} M_k(K_k)\boldsymbol{e}_3 = \sum_{k\in\mathcal{C}_b} s_k \boldsymbol{f}_k \times \boldsymbol{e}_b + \sum_{k\in\mathcal{C}_b} z_k \boldsymbol{f}_k \times \boldsymbol{e}_3 & \text{(17b)} \end{cases}$$

noting $\boldsymbol{G}_b\boldsymbol{K}_k = s_b\boldsymbol{e}_b + z_b\boldsymbol{e}_3$. In Eq. (17b), it is easy to show that the second term on the right-hand side is negligible compared to the first one $[d_{\min}/l = \mathcal{O}(\epsilon^2)]$. Hence, the equilibrium of bundle b can be approximated by

$$\forall b, \quad \begin{cases} \displaystyle\sum_{k\in\mathcal{C}_b} \boldsymbol{f}_k = \boldsymbol{0} & \text{(18a)} \\ \displaystyle\sum_{k\in\mathcal{C}_b} m_k \boldsymbol{e}_3 = \sum_{k\in\mathcal{C}_b} \epsilon\, s_k^* \boldsymbol{f}_k \times \boldsymbol{e}_b. & \text{(18b)} \end{cases}$$

As contact forces are contained in $\mathcal{P}$ and functions of $\Delta\tilde{\boldsymbol{v}}_k$ only, it is worth noting that the above-noted momentum balances simplify in a two-dimensional mechanical problem. Equation (18a) presents vectorial equations contained in $\mathcal{P}$ and Eq. (18b) presents vectorial equations along $\boldsymbol{e}_3$.

III. UPSCALING: DETERMINATION OF THE MACROSCOPIC BEHAVIOR

To determine the macroscopic behavior of such planar bundle networks, Le Corre *et al.* (2004) have recently used the homogenization method for periodic discrete structures. This theoretical framework is an extension to discrete structures of the homogenization method of multiple scale expansions for periodic structures (Auriault, 1991; Bensoussan *et al.*, 1978; Sanchez-Palencia, 1980). It has been initially developed for the modeling of mechanical properties of trusses, honeycomb structures or buildings in the scope of elasticity (Boutin and Hans, 2003; Moreau and Caillerie, 1995, 1998; Pradel and Sab, 1998; Tollenaere and Caillerie, 1998). Its principal advantages rely upon the possibility of avoiding prerequisites at the macroscopic scale, modeling finite size macroscopic samples, determining whether discrete systems can be homogenized or not, providing the domains of validity of the macroscopic models (Auriault, 1991). The objective of the following sections is to give a brief review of the derivation of $\boldsymbol{\sigma}^{(f)}$ by this upscaling technique. For details related to the theoretical aspects of the analysis given in the following, the reader is referred to Le Corre *et al.* (2004).

A. Methodology

The homogenization method is based on the periodicity assumption (see Fig. 1). As a consequence, the suspension is seen as a periodic assembly of identical representative elementary volumes (REVs), each REV containing N bundles b connected through C bundle-bundle connections k. Combined with the scale separation condition (3), the periodicity condition enables one to write the translational and rotational velocity fields $\tilde{\boldsymbol{v}}_b$ and ϕ_b of a given bundle b in "discrete" asymptotic expansions in powers of the scale separation parameter ϵ such as (Le Corre *et al.*, 2004; Moreau and Caillerie, 1995; Tollenaere and Caillerie, 1998)

$$\tilde{\boldsymbol{v}}_b(\tilde{\boldsymbol{x}}) = \tilde{\boldsymbol{v}}_b^{[0]}(\tilde{\boldsymbol{x}}) + \epsilon\,\tilde{\boldsymbol{v}}_b^{[1]}(\tilde{\boldsymbol{x}}) + \epsilon^2\tilde{\boldsymbol{v}}_b^{[2]}(\tilde{\boldsymbol{x}}) + \cdots, \tag{19}$$

$$\phi_b(\tilde{\boldsymbol{x}}) = \phi_b^{[0]}(\tilde{\boldsymbol{x}}) + \epsilon\,\phi_b^{[1]}(\tilde{\boldsymbol{x}}) + \epsilon^2\phi_b^{[2]}(\tilde{\boldsymbol{x}}) + \ldots. \tag{20}$$

In these equations, fields $\tilde{\boldsymbol{v}}_b^{[n]}$ (respectively, $\phi_b^{[n]}$) which denote the "ϵ^n-order" fluctuation of $\tilde{\boldsymbol{v}}_b$ (respectively, ϕ_b), as depicted in Fig. 1, are continuous functions of the space variable $\tilde{\boldsymbol{x}}$ and periodic function of the local bundle index b. These expansions are then introduced in the momentum balance equations (18a) and (18b) and the use of a virtual power formulation is made in order to determine the macroscopic behavior of the considered fiber networks (Tollenaere and Caillerie, 1998). In particular, studying the self equilibrium of a REV at the lower orders of ϵ, Le Corre *et al.* have shown that velocity fields $\tilde{\boldsymbol{v}}_b^{[0]}$ do not depend on the considered bar b, so that

$$\forall b, \quad \tilde{\boldsymbol{v}}_b^{[0]} = \tilde{\boldsymbol{v}}^{(s)}. \tag{21}$$

B. Constitutive equations

To determine the nature of the macroscopic behavior of a network of bundles whose bundle equilibrium is driven by the two-dimensional (2D) momentum balances (18a) and (18b), we have considered three situations, depending on the order of magnitude of interaction moments [the left-hand side of Eq. (18b)] with respect to moments of interaction forces [the right-hand side of Eq. (18b)], i.e., $\mathcal{O}(\epsilon^{-1}), \mathcal{O}(1)$, and $\mathcal{O}(\epsilon)$. In the first case, when local interaction moments are of one order of magnitude greater than moments of interaction forces, the resulting equivalent macroscopic medium of the bundle network is a general Cosserat medium (Cosserat and Cosserat, 1909; Germain, 1973; Truesdell and Noll, 1965). In the two other situations, i.e., when local interactions moments are of the same order of magnitude, or of one order of magnitude smaller than the moments of interaction forces, the suspension is a usual Cauchy medium.

We will suppose that the considered bundle networks belong to the third situation : (i) at the macroscopic scale, they behave as usual Cauchy media and (ii) their bundle-bundle contacts are such that interactions moments are small $[\mathcal{O}(\epsilon)]$ with respect to the moments of interaction forces. This assumption will be extensively discussed and validated *a posteriori* in Sec. VI. Notice that in this situation, the macroscopic Cauchy 2D stress tensor $\tilde{\boldsymbol{\sigma}}^{(f)}$ is defined within a relative error of $\mathcal{O}(\epsilon)$ as

$$\tilde{\boldsymbol{\sigma}}^{(f)} = \frac{1}{V^{(s)}}\sum_{k=1}^{C} \tilde{\boldsymbol{\xi}}_k \otimes \tilde{\boldsymbol{f}}_k^{[0]}. \tag{22}$$

In Eq. (22) $V^{(s)}$ is the volume of the considered REV, $\tilde{\boldsymbol{\xi}}_k$ is the projection of $\boldsymbol{G}^b\boldsymbol{G}^c$ in plane $\mathcal{P}$, and $\tilde{\boldsymbol{f}}_k^{[0]}$ is the first non-null term in the asymptotic expansion of the interaction force $\tilde{\boldsymbol{f}}_k$.

C. Essential properties of the equivalent continuum

The stress tensor $\tilde{\boldsymbol{\sigma}}^{(f)}$ can be proved to be symmetric, but as is clear from Eq. (22), enters in the scope of general anisotropy. Its explicit calculation requires the determination of forces $\tilde{\boldsymbol{f}}_k^{[0]}$ given by

$$\tilde{\boldsymbol{f}}_k^{[0]} = \mu_k \|\Delta\tilde{\boldsymbol{v}}_k^{[1]}\|^{m-1}\Delta\tilde{\boldsymbol{v}}_k^{[1]}, \tag{23}$$

where

$$\Delta\tilde{\boldsymbol{v}}_k^{[1]} = \tilde{\boldsymbol{v}}_c^{[1]} - \tilde{\boldsymbol{v}}_b^{[1]} + \tilde{\boldsymbol{L}}^{(s)} \cdot \tilde{\boldsymbol{\xi}}_k + s_c^* \phi_c^{[0]} \boldsymbol{e}_3 \times \boldsymbol{e}_c - s_b^* \phi_b^{[0]} \boldsymbol{e}_3 \times \boldsymbol{e}_b. \tag{24}$$

Moreover, as explained in Le Corre *et al.* (2004), kinematic unknowns $\tilde{\boldsymbol{v}}_b^{[1]}$ and $\phi_b^{[0]}$ can be calculated by considering $\tilde{\boldsymbol{L}}^{(s)}$ as input data of the nonlinear self-equilibrium problem of the REV that contains N bundles:

$$\forall\ b \in V^{(s)},\quad \begin{cases} \displaystyle\sum_{k \in \mathcal{C}_b} \tilde{\boldsymbol{f}}_k^{[0]}(\tilde{\boldsymbol{v}}_b^{[1]}, \tilde{\boldsymbol{v}}_c^{[1]}, \phi_b^{[0]}, \phi_c^{[0]}, \tilde{\boldsymbol{L}}^{(s)}) = \boldsymbol{0} \\ \displaystyle\sum_{k \in \mathcal{C}_b} m_k^{[0]} \boldsymbol{e}_3 + \sum_{k \in \mathcal{C}_b} s_b^* \boldsymbol{e}_b \times \tilde{\boldsymbol{f}}_k^{[0]}(\tilde{\boldsymbol{v}}_b^{[1]}, \tilde{\boldsymbol{v}}_c^{[1]}, \phi_b^{[0]}, \phi_c^{[0]}, \tilde{\boldsymbol{L}}^{(s)}) = \boldsymbol{0} \end{cases} \tag{25}$$

noting

$$m_k^{[0]} = \beta_k \left| \phi_c^{[0]} - \phi_b^{[0]} \right|^{m-1} (\phi_c^{[0]} - \phi_b^{[0]}). \tag{26}$$

Following this procedure and assuming that no internal mechanism is likely to occur i.e., no isolated fibers or groups of fibers), a well-posed problem is obtained, with $3N$ equations for $3N$ unknowns. Isolated fibers do not influence the overall equilibrium of the network so they can be removed from the assembly by a simple numerical treatment. Practically, for the bundle geometry and the REVs we have generated (see Sec. IV), the maximum number of eliminated bundles was about 3 for the lowest tested fiber fractions $f^{(f)} = 0.07$, which represents at most 1.5% of the total number of bundles. This procedure enables one to analyze rather "low" fiber contents while staying in the concentrated regime. In our numerical studies described in the following, the case of isolated groups of fibers was never encountered, it could certainly happen at yet lower fiber volume fractions. Such a case was not investigated here because it would enter in the domain of semidilute suspensions, where the matrix contribution cannot be neglected anymore.

Under this restrictive assumption, Eq. (25) enables the calculation of $\tilde{\boldsymbol{v}}_b^{[1]}$ and $\phi_b^{[0]}$ for any given imposed macroscopic velocity gradient. This equilibrium can be set in the following general form:

$$\mathbf{F}(\mathbf{X}, \tilde{\boldsymbol{L}}^{(s)}) = \mathbf{0}, \tag{27}$$

$\mathbf{X}$ being a vector of size $3N$ containing all the local kinematic unknowns. In this system, $\tilde{\boldsymbol{\sigma}}^{(f)}$ is an implicit nonlinear function of $\tilde{\boldsymbol{L}}^{(s)}$, which actually reduces to a function of the macroscopic strain rate tensor $\tilde{\boldsymbol{D}}^{(s)}$ because of the symmetry of stresses. Furthermore, the following property can be shown (Le Corre *et al.*, 2004):

$$\left| \begin{array}{l} \textit{if } \mathbf{X} \textit{ is the solution of } \mathbf{F}(\mathbf{X}, \tilde{\mathbf{L}}^{(s)}) = \mathbf{0}, \\ \lambda\mathbf{X} \textit{ is the solution of } \mathbf{F}(\mathbf{X}', \lambda\tilde{\boldsymbol{L}}^{(s)}) = \mathbf{0}. \end{array} \right. \tag{28}$$

As a direct consequence:

$$\forall \lambda \in \mathbb{R} \quad \tilde{\boldsymbol{\sigma}}^{(f)}(\lambda \tilde{\boldsymbol{D}}^{(s)}) = \lambda |\lambda|^{m-1} \tilde{\boldsymbol{\sigma}}^{(f)}(\tilde{\boldsymbol{D}}^{(s)}), \tag{29}$$

so that the macroscopic stress tensor $\tilde{\boldsymbol{\sigma}}^{(f)}$ exhibits a degree m homogeneity with respect to $\tilde{\boldsymbol{D}}^{(s)}$. Consequently, the studied suspension is an anisotropic power-law fluid, with a macroscopic power-law index m, which is equal to the one postulated at the level of bundle-bundle interactions.

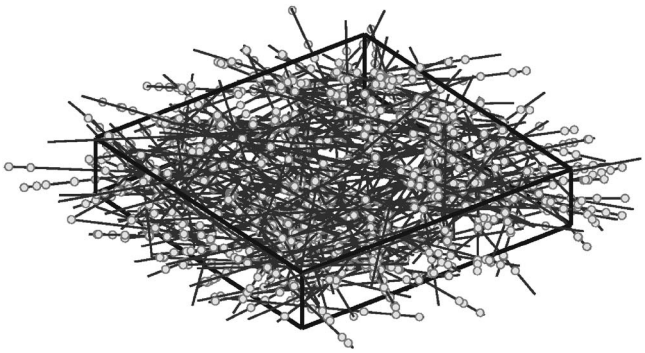

FIG. 4. Example of generated representative elementary volume ($V^{(s)}=25\times25\times2.5$ mm^3), containing 437 bundles of length 25 mm ($f^{(f)}=0.188$). Open circles represent the connections location, lines represent the centerline of the bundles ($\delta^*=3$).

IV. NUMERICAL PROBLEM

The objective of this section is to show how it is possible to highlight more precisely the influence of the microstructure of the bundle network on the macroscopic behavior. For that purpose, we consider the deformation of bundle networks as representative as possible of typical industrial compression molded composites (Sec. IV A). The quantitative responses of such microstructures, i.e., the macroscopic stress state $\tilde{\boldsymbol{\sigma}}^{(f)}$ and the evolution of the orientation of bundles to given imposed mechanical loadings, i.e., the macroscopic strain rate $\tilde{\boldsymbol{L}}^{(s)}$, are studied through a numerical approach (Sec. IV B).

A. Microstructure generation

The morphology of real bundle networks is something roughly complex that can hardly be described with precision. Micrographies of bundles configuration in industrial parts can be achieved by several experimental observation techniques such as X-rays or microscopy, (Greene and Wilkes, 1997; Hamada *et al.*, 1994). Those techniques eventually enable one to obtain precise data about the spatial distribution of bundles position and orientation, but still do not provide any data about the connectivity of bundles. An alternate way to obtain fully defined bundle networks is to use numerical generation processes that try to mimic real microstructures. Such a method plants the problem of the representativity of the generated microstructure with respect to the original one. Fortunately, industrial polymer composites such as SMC and GMT involve very concentrated planar fiber suspensions, so an elementary representative volume will contain a great number of bundles. In this idea, a statistically equivalent microstructure might be quite easily found and a random generation method seems appropriate.

1. Processing

Three-dimensional networks containing N bundles (see Fig. 4) were generated. The center of mass of each bundle has a random position (x_b,y_b) in the plane $\mathcal{P}$ ranging in $[-d/2,d/2]$, and a random altitude h_b in $[0,h]$, d and h being, respectively, the dimensions of the REV in the $(\boldsymbol{e}_1,\boldsymbol{e}_2)$ plane and in the $\boldsymbol{e}_3$ direction (thickness of the sheets). Quasi-isotropic and oriented planar networks are generated using, respectively, a uniform distribution of angles θ_b, and a Gaussian random distribution of angles θ_b centered on $\theta=0$ and with a variable standard deviation. The last procedure enables the generation of bundle networks having almost isotropic orientations to almost unidirectional ones.

The connectivity of the network, that is to say the location of the C bundle-bundle contact points is computed using a deterministic methodology directly inspired by the statistical tube model proposed in previous studies (Doi and Edwards, 1978; Ranganathan and Advani; 1991; Toll, 1993) and already used in rheological models of highly concentrated planar fiber suspensions (Servais *et al.*, 1999a, b; Toll and Månson, 1994). For that purpose, a control volume V_b is defined around each considered bundle b. Every bundle c whose centerline intersects V_b is added to the connectivity set of bundle b, denoted $\mathcal{C}_b$. The control volume V_b is chosen as a rectangular box with dimensions $l \times d_{\max} \times \delta^* d_{\min}$, where δ^* is a dimensionless parameter. Its determination will be detailed in Sec. V B, when comparing the prediction of the model with experimental data.

2. Macroscopic characterization of generated networks

At the macroscopic level, the generated bundle networks are first characterized by their orientational state, which can be defined in different manners. The most descriptive approach would be to use the orientation distribution function Ψ (Folgar *et al.*, 1984). However, to our knowledge, it can hardly be determined without cumbersome calculations that are not possible in practical applications. Instead, one prefers to use compact and convenient approximations of Ψ, such as the second-order orientation tensor $\tilde{\boldsymbol{A}}$ (Advani and Tucker, 1987):

$$\tilde{\boldsymbol{A}} = \frac{1}{N}\sum_{b=1}^{N} \boldsymbol{e}_b \otimes \boldsymbol{e}_b. \tag{30}$$

As shown in Fig. 5, such a compact macroscopic measurement of bundles orientation gives a reasonable approximation Ψ_A (Advani and Tucker, 1987) of the orientation distribution function Ψ in the particular case of the studied microstructures:

$$\Psi_A(\theta) = \frac{1}{\pi} + \frac{4}{\pi}\left(\tilde{\boldsymbol{A}} - \frac{1}{2}\tilde{\boldsymbol{\delta}}\right) : \left(\boldsymbol{e}_\theta \otimes \boldsymbol{e}_\theta - \frac{1}{2}\tilde{\boldsymbol{\delta}}\right), \tag{31}$$

where $\boldsymbol{e}_\theta = \cos\theta \boldsymbol{e}_1 + \sin\theta \boldsymbol{e}_2$ is the vector corresponding to orientation θ. Note that the discrete representation of the distribution functions Ψ plotted in Fig. 5 were built starting from the initial normal distributions of orientation (cf. Sec. IV A 1), and then using the π-periodicity of Ψ with respect to θ in order to renormalize the resulting histograms.

The generated bundle networks are also characterized by the volume fraction of bundles $f^{(f)}$, related to the number of bundles per unit volume $n^{(f)}$:

$$f^{(f)} = \frac{\pi}{4} l d_{\max} d_{\min} n^{(f)} \text{ with } n^{(f)} = \frac{N}{V^{(s)}}. \tag{32}$$

One can also introduce the number of connections per unit volume $c^{(f)}$:

$$c^{(f)} = \frac{C}{V^{(s)}} = \frac{1}{2} n^{(f)} n_{c/b}, \tag{33}$$

where $n_{c/b}$ is the local average number of connections per bundle. Using the chosen control volume in the tube model framework proposed by Toll (1993), $n_{c/b}$ is theoretically given by

$$n_{c/b} = n^{(f)} l \delta^* (l d_{\min} \phi_1 + d_{\max} d_{\min} \phi_2 + d_{\max} d_{\min}). \tag{34}$$

Using Eqs. (32)–(34), $c^{(f)}$ may also be expressed as

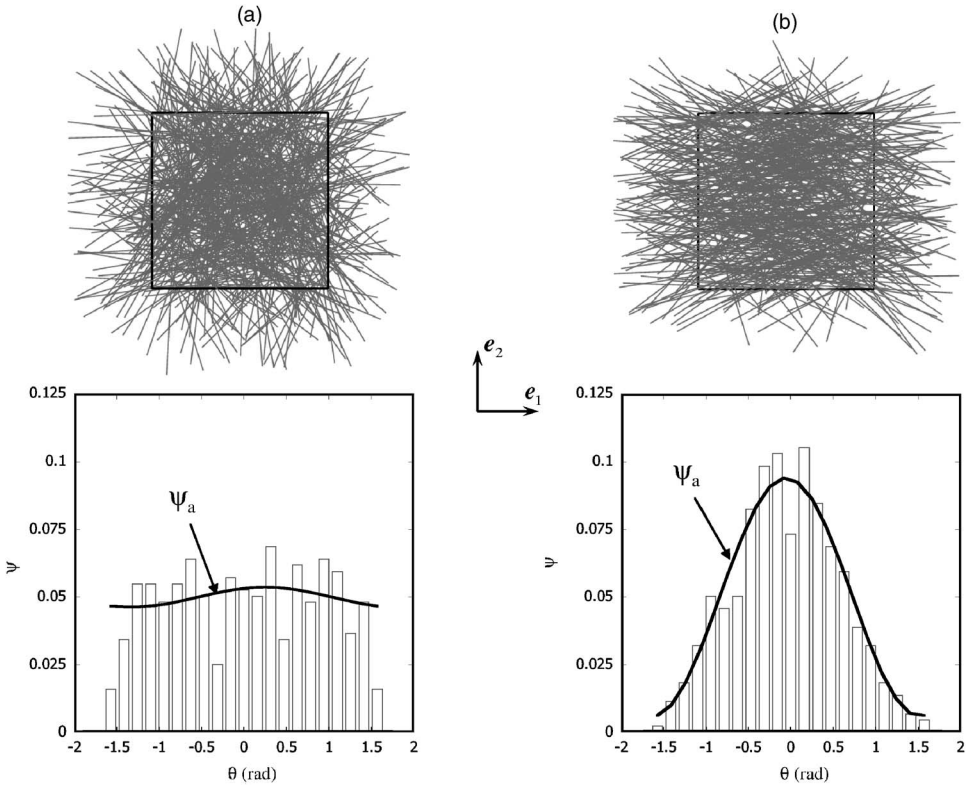

FIG. 5. Approximation Ψ_A of the orientation distribution function Ψ given by the second-order orientation tensor $\widetilde{\boldsymbol{A}}$ in the case of a quasi-isotropic microstructure (A_{11}=0.501, A_{22}=0.499, A_{12}=0) (a), and of an oriented microstructure (A_{11}=0.7, A_{22}=0.3, A_{12}=0) (b).

$$c^{(f)} = \frac{8{f^{(f)}}^2}{\pi^2 l d_{\max} d_{\min}} \delta^* \left(\frac{l}{d_{\max}} \phi_1 + \phi_2 + 1 \right). \tag{35}$$

Subsequently, the average number of connection $n_{c/b}$ and the density of connection $c^{(f)}$ are, respectively, linear and square functions of the fiber volume fraction $f^{(f)}$.

The 2D-orientation functions ϕ_1 and ϕ_2 go from 0 to $2/\pi$ and from 1 to $2/\pi$ when the planar bundle orientation goes from fully aligned to random, respectively (Toll, 1993). In the current determinist approach, they were simply calculated in the following discrete way:

$$\phi_1 = \frac{1}{N^2} \sum_{b=1}^{N} \sum_{c=1}^{N} |\sin(\theta_b - \theta_c)|, \tag{36}$$

$$\phi_2 = \frac{1}{N^2} \sum_{b=1}^{N} \sum_{c=1}^{N} |\cos(\theta_b - \theta_c)|. \tag{37}$$

In Fig. 6, functions ϕ_1 and ϕ_2 were plotted in terms of A_I, the major eigenvalue of $\widetilde{\boldsymbol{A}}$. They were computed in a discrete way [Eqs. (36) and (37)] for several orientation distributions going from the isotropic state (A_I=0.5) to the perfectly aligned state (A_I=1). As visible from Eqs. (35) and (41) (see Sec. IV C), approximating these structural descrip-

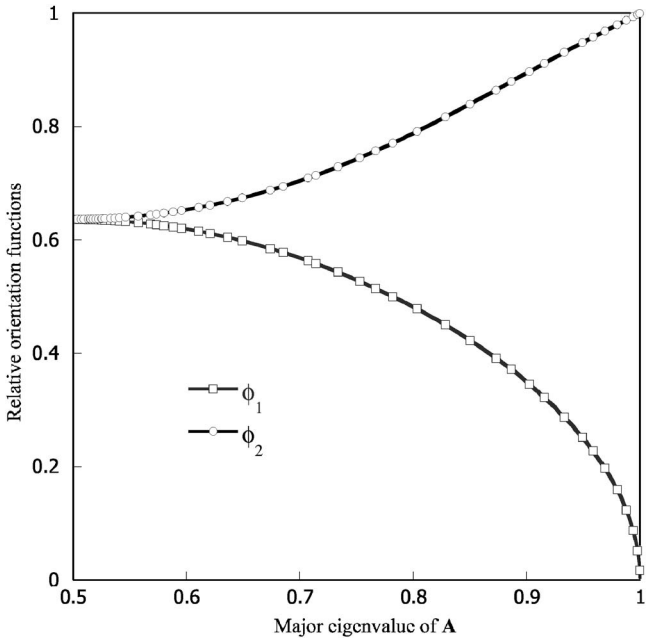

FIG. 6. Evolution of the relative orientation functions ϕ_1 and ϕ_2 with the major eigenvalue of the second order orientation tensor $\widetilde{\boldsymbol{A}}$.

tors as functions of A_I could be a convenient way of incorporating the present results into a continuum model of orientation and rheology.

3. Analysis of the generation procedure

In order to validate our numerical generation procedure, microstructures with identical bundles (l=25 mm, $d_{\min}$=0.06 mm, $d_{\max}$=0.6 mm, δ^*=3), orientation tensor $\widetilde{\boldsymbol{A}}$, fiber volume fraction $f^{(f)}$, but with an increasing number of bundles N were generated (as the number of bundles N was increased, the height h of $V^{(s)}$ was increased). The computed density of connections $c^{(f)}$ was then compared to the one given by the analytical predictions of the statistical tube model (Toll, 1993). For that purpose, the theoretical average number of connections per bundle $n_{c/b}$ was estimated from the generated angular positions through Eqs. (34)–(37).

Within the investigated fiber volume fraction and orientation ranges ($0.07 \leqslant f^{(f)} \leqslant 0.25$, $0 \leqslant A_{11} \leqslant 0.9$), results show that for $N > 400$ bundles, a fairly good correlation is obtained between the current determinist algorithm and the statistical tube model: $\Delta c^{(f)}/c^{(f)} \pm 5\%$. Therefore, in order to analyze the rheology of statistically representative microstructures, calculations presented in the next sections were systematically performed with a minimum number of bundles of 400.

B. Numerical rheometry experiments

Given the generated REVs and the physics of bundle-bundle interactions, it is now clear from the above-mentioned considerations that the rheology of the studied suspensions can be computed by the means of a procedure of *numerical rheometry experiments*. Such numerical experiments consist in the following steps

(1) Imposing a macroscopic velocity gradient $\widetilde{\boldsymbol{L}}^{(s)}$ to the generated REVs. As suspensions are assumed incompressible and as $L_{i3}=L_{3i}=0$ $(i=1,2)$, this is equivalent to imposing $\boldsymbol{L}^{(s)}$ since the incompressibility yields $L_{11}^{(s)}+L_{22}^{(s)}+L_{33}^{(s)}=0$.

(2) Solving numerically the system (27). This was achieved using a classical Newton-Raphson method based on successive corrections $\boldsymbol{\delta}\mathbf{X}$ of the vector $\mathbf{X}$ such as

$$\frac{\partial \mathbf{F}}{\partial \mathbf{X}}(\mathbf{X},\widetilde{\mathbf{L}}^{(s)})\cdot\boldsymbol{\delta}\mathbf{X}=-\mathbf{F}(\mathbf{X},\widetilde{\boldsymbol{L}}^{(s)}). \tag{38}$$

As expected, the convergence was found to be hardest as the power-law exponent m decreased. Unfortunately, due to the stiffness of such a nonlinear problem, it became almost impossible for $m<0.1$, so very low sensitivities could not be investigated.

C. Post-treatment of results

Given the macroscopic loading path $\widetilde{\boldsymbol{L}}^{(s)}$, the solution of the system (27), composed of kinematic fields $\widetilde{\boldsymbol{v}}_b^{[1]}$ and $\phi_b^{[0]}$, finally allows the computation of the following data

(1) The rate $\dot{\widetilde{\boldsymbol{A}}}$ of the orientation tensor $\widetilde{\boldsymbol{A}}$ defined as

$$\dot{\widetilde{\boldsymbol{A}}}=\frac{1}{N}\sum_{b=1}^{N}\dot{\boldsymbol{e}}_b\otimes\boldsymbol{e}_b+\boldsymbol{e}_b\otimes\dot{\boldsymbol{e}}_b=\frac{1}{N}\sum_{b=1}^{N}(\boldsymbol{\omega}_b\times\boldsymbol{e}_b)\otimes\boldsymbol{e}_b+\boldsymbol{e}_b\otimes(\boldsymbol{\omega}_b\times\boldsymbol{e}_b). \tag{39}$$

Due to property (28), it follows that $\dot{\widetilde{\boldsymbol{A}}}$ is an homogeneous function of degree 1 with respect to $\widetilde{\boldsymbol{L}}^{(s)}$:

$$\forall\lambda\in\mathbb{R}\quad\dot{\widetilde{\boldsymbol{A}}}(\lambda\widetilde{\boldsymbol{L}}^{(s)})=\lambda\dot{\widetilde{\boldsymbol{A}}}(\widetilde{\boldsymbol{L}}^{(s)}). \tag{40}$$

(2) The macroscopic planar stress tensor $\widetilde{\boldsymbol{\sigma}}^{(f)}$ using Eq. (22)–(24). Note that in the particular case of the generated bundle networks which follows the statistical tube model of Toll, a more interesting expression of $\widetilde{\boldsymbol{\sigma}}^{(f)}$ can be established, accounting for (13), (22)–(24), and (35) and noting $\widetilde{\boldsymbol{\xi}}_k^{*}=\widetilde{\boldsymbol{\xi}}_k/l$:

$$\widetilde{\boldsymbol{\sigma}}^{(f)}=\eta_{(e)}\frac{\delta^{*}}{\alpha^{m}}\frac{8{f^{(f)}}^{2}}{\pi^{2}}\frac{d_{\max}}{d_{\min}}\left(\frac{l}{d_{\max}}\phi_1+\phi_2+1\right)\frac{1}{C}\sum_{k=1}^{C}\frac{\|\Delta\widetilde{\boldsymbol{v}}_k^{[1]}\|^{m-1}}{|\sin\Delta\theta_k|}\widetilde{\boldsymbol{\xi}}_k^{*}\otimes\Delta\widetilde{\boldsymbol{v}}_k^{[1]}, \tag{41}$$

ϕ_1 and ϕ_2 being given by Eqs. (36) and (37), respectively. Equation (41) clearly underlines the role of the bundles geometry $(d_{\min}/d_{\max},d_{\max}/l)$, the fiber volume fraction $(f^{(f)})$, the orientation of network (ϕ_1,ϕ_2), the rheology of the entrapped fluid $(\eta_{(e)},m)$, the geometry of the contact zones $(\alpha,|\sin\Delta\theta_k|)$ and the external loading $(\Delta\widetilde{\boldsymbol{v}}_k^{[1]}(\widetilde{\boldsymbol{L}}^{(s)}))$, on the overall stress state $\widetilde{\boldsymbol{\sigma}}^{(f)}$.

(3) The macroscopic stress tensor of the suspension $\boldsymbol{\sigma}^{(s)}$: according to the basic assumptions detailed in Secs. II B and II C, i.e., Eq. (2), $L_{i3}=L_{3i}=0$ $(i=1,2)$ and $\boldsymbol{f}_k\cdot\boldsymbol{e}_3=0$, the 3D extension of the 2D analysis we propose is very simple and straightforward:

$$\boldsymbol{\sigma}^{(s)}=-p\boldsymbol{\delta}+\widetilde{\boldsymbol{\sigma}}^{(f)}=\begin{bmatrix}-p+\widetilde{\sigma}_{11}^{(f)} & \widetilde{\sigma}_{12}^{(f)} & 0\\ \widetilde{\sigma}_{12}^{(f)} & -p+\widetilde{\sigma}_{22}^{(f)} & 0\\ 0 & 0 & -p\end{bmatrix}_{\boldsymbol{e}_1,\boldsymbol{e}_2,\boldsymbol{e}_3}. \tag{42}$$

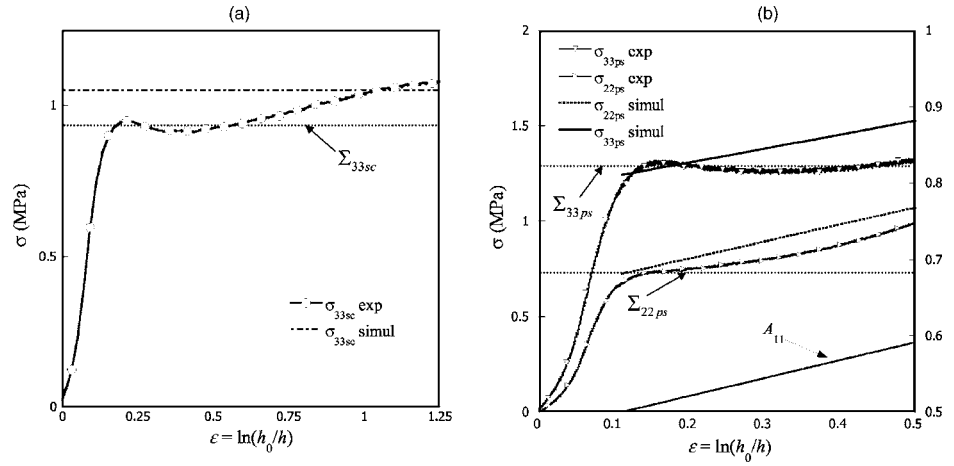

FIG. 7. Typical experimental response of SMC of fiber content $f^{(f)}=0.188$ (Dumont *et al.*, 2003): simple compression test (a) and a plane strain compression test (b), both performed at an axial strain rate $D_{33}=0.01\ s^{-1}$-Comparison with the results of the micro-macro model.

V. COMPARISON WITH EXPERIMENTS

A. Previous experimental studies

In previous experimental works, the rheology of an industrial SMC was analyzed under various homogeneous testing conditions (Dumont *et al.*, 2003; Le Corre *et al.*, 2002). The tested material was standard SMC (LP 606) supplied by Mecelec Composite and Recyclage (Tournon, France). Produced sheets were made of a polyester-based paste matrix (19.6wt % of polyester resin, 1.56wt % of styren, 62.07wt % of mineral charge of $CaCO_3$ of mean diameter 2 μm, 16.77wt % of other additives) and glass fiber bundles (length $l=25$ mm, cross sections corresponding to those sketched in Fig. 2) that were randomly oriented in the plane of the 2.5 mm-thick sheets. For that purpose, a specific rheometer was developed allowing one to perform homogeneous simple compression (sc), plane strain compression (ps) (i.e., the suspension is constrained to flow inside a channel) and shear tests at room temperature, for a wide range of constant imposed strain rates (from 10^{-3} to 1 s^{-1}) and volume fractions of bundles $f^{(f)}$ (from 0.035 to 0.188). The samples used with such rheometers were sufficiently large to avoid possible size effects induced by the length of the bundles. In the following, we will only be interested in results obtained in simple and plane strain compression tests. For these two homogeneous testing conditions, assuming (i) incompressibility and (ii) initial in-plane isotropy of the sheets, the homogeneous stress and strain rate tensors are

$$\boldsymbol{\sigma}^{(s)} = \sigma^{(s)}_{33\mathrm{sc}}\boldsymbol{e}_3 \otimes \boldsymbol{e}_3, \quad \boldsymbol{D}^{(s)} = D^{(s)}_{33}(-\tfrac{1}{2}\boldsymbol{e}_1 \otimes \boldsymbol{e}_1 - \tfrac{1}{2}\boldsymbol{e}_2 \otimes \boldsymbol{e}_2 + \boldsymbol{e}_3 \otimes \boldsymbol{e}_3) \tag{43}$$

and

$$\boldsymbol{\sigma}^{(s)} = \sigma^{(s)}_{22\mathrm{ps}}\boldsymbol{e}_2 \otimes \boldsymbol{e}_2 + \sigma^{(s)}_{33\mathrm{ps}}\boldsymbol{e}_3 \otimes \boldsymbol{e}_3, \quad \boldsymbol{D}^{(s)} = D^{(s)}_{33}(-\boldsymbol{e}_1 \otimes \boldsymbol{e}_1 + \boldsymbol{e}_3 \otimes \boldsymbol{e}_3) \tag{44}$$

during the simple compression (sc) and plane strain compression (ps) experiments, respectively. Typical results obtained from (sc) and (ps) experiments are given in Fig. 7. The graphs plotted in this figure show the axial stresses $\sigma^{(s)}_{33\mathrm{sc}}, \sigma^{(s)}_{33\mathrm{ps}}$, and lateral stress $\sigma^{(s)}_{22\mathrm{ps}}$, as functions of the axial Hencky strain $\varepsilon_{33}=\ln(h_0/h)$, h_0 and h being the initial and current thickness of the sheets. Note that for the rest of the document, compressive

stresses, strain-rates and strains will be taken as positive. Stresses first exhibit a sharp increase and rapidly reach a threshold stress denoted Σ_{ii}, directly deduced from the $(\sigma - \varepsilon)$ curves presented in Fig. 7: during this stage, air as well as styrene entrapped inside the SMC is expelled, and the initial wavy surface of the sheets is flattened. From the threshold stress, the SMC effectively starts to flow in the rheometer: in the following, we will analyze results from these threshold stresses. Experimental results are summarized in the following

(1) Threshold stresses are power-law functions of the axial imposed strain rate D_{33}. Introducing D_0 a characteristic strain rate of 1 s^{-1}, this yields to

$$\Sigma^{(s)}_{33\mathrm{sc}} = \eta_{33\mathrm{ps}}\left(\frac{D^{(s)}_{33}}{D_0}\right)^{n-1} D^{(s)}_{33} \text{ in simple compression,} \tag{45}$$

$$\begin{aligned}\Sigma^{(s)}_{33\mathrm{ps}} &= \eta_{33\mathrm{ps}}\left(\tfrac{D^{(s)}_{33}}{D_0}\right)^{n-1} D^{(s)}_{33} \\ \Sigma^{(s)}_{22\mathrm{ps}} &= \eta_{22\mathrm{ps}}\left(\tfrac{D^{(s)}_{33}}{D_0}\right)^{n-1} D^{(s)}_{33}\end{aligned} \text{ in plane strain compression.} \tag{46}$$

(2) Whatever the deformation mode [(sc) or (ps)], the investigated bundle contents (except for the bulk matrix) and imposed strain rates, the power-law exponent n takes a constant value of 0.44 at room temperature.

(3) For strain rates ranging from 10^{-3} to 10 s^{-1}, the stress levels recorded for the bulk pasty matrix (without bundles) were also power-law functions of the strain rate (Le Corre *et al.*, 2002), but with a power-law exponent of 0.58. Such a difference between the bulk matrix and the SMCs could be explained by the arguments developed in Sec. II C 3 (power-law valid only within a restricted strain rate range, structural changes or particle size effects affecting the rheology of the pasty matrix in the entrapped zones).

(4) The threshold viscosities $\eta_{33\mathrm{sc}}$, $\eta_{33\mathrm{ps}}$, and $\eta_{22\mathrm{ps}}$ strongly depend on the bundle content, those dependencies being well described by the following second-order polynomial functions:

$$\frac{\eta_{33\mathrm{sc}}}{\eta_{\mathrm{ref}}} = 0.86 + 86f^{(f)} + 860f^{(f)^2}, \tag{47}$$

$$\frac{\eta_{33\mathrm{ps}}}{\eta_{\mathrm{ref}}} = 1 + 98f^{(f)} + 980f^{(f)^2}, \tag{48}$$

$$\frac{\eta_{22\mathrm{ps}}}{\eta_{\mathrm{ref}}} = 0.5 + 67f^{(f)} + 670f^{(f)^2}, \tag{49}$$

where η_{ref}=0.18 MPa.s is the measured axial viscosity of the polymer matrix ($f^{(f)}=0$) for a plane strain compression test.

(5) During the deformation, stress $\sigma^{(s)}_{33\mathrm{sc}}$ remains approximately constant during the (sc) experiments, whereas for the (ps) experiments, a slight increase of the stresses $\sigma^{(s)}_{33\mathrm{ps}}$ and $\sigma^{(s)}_{22\mathrm{ps}}$ is observed (see Fig. 7).

B. Identification of the model parameters

In order to compare the previous experimental results with the predictions of the micro-macro approach, various REVs similar to those depicted in Fig. 5 were first gen-

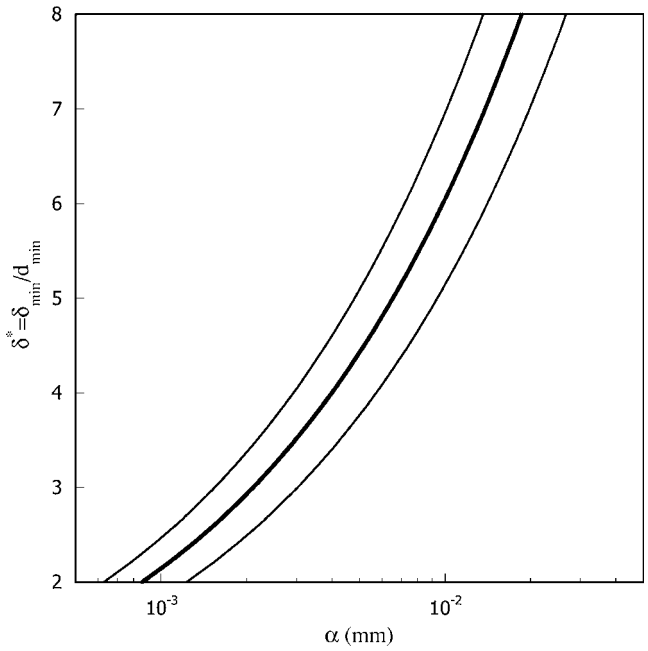

FIG. 8. Admissible range of values of parameters α and δ^* determined from a unique simple compression test (Dumont *et al.*, 2003; Le Corre *et al.*, 2002).

erated with the appropriate bundle geometry parameters ($l, d_{\min}$, and $d_{\max}$), contents $f^{(f)}$ and with random planar orientations, following the generation procedure summarized in Sec. IV A. Then, in accordance with property (29), the power-law exponent m of the viscous local interaction efforts (13) and (16) was set to 0.44, i.e., the power law exponent n observed at the macroscopic level. Moreover, the shear viscosity of the entrapped matrix $\eta_{(e)}$ was arbitrarily set to 0.055 MPa s: this value is consistent with that obtained during rheometry experiments performed on the paste matrix (Dumont *et al.*, 2003; Le Corre *et al.*, 2002).

The two remaining constitutive parameters to be identified are α, the averaged sheared thickness, and δ^*, the parameter that governs the height of the control volume for the determination of the density of connections inside the suspension. As evident from Eq. (41), both have an influence on the computed stresses: the influence of α on $\boldsymbol{\sigma}^{(s)}$ is $\mathcal{O}(1/\alpha^m)$, whereas δ^* increases the stresses in a linear way. Figure 8 represents the range of admissible couples (α, δ^*) that induce a predicted threshold stress identical to that recorded during a simple compression experiment achieved on a SMC sample, i.e., $\Sigma_{33\text{sc}}$ ($f^{(f)}=0.188$, $D_{33}^{(s)}=-0.01\ \text{s}^{-1}$). To determine this surface, a first arbitrary guess of the sheared thickness α_0 was fixed to 5×10^{-3} mm. Its associated parameter $\delta_0^*=4$ was then determined by simple identification of the predicted threshold stress $\sigma_{33\text{sc}0}$ with the experimental one. From this first admissible couple (α_0, δ_0^*), one can deduce all the other admissible couples (α, δ^*) by

$$\delta^* = \frac{\sigma_{33\text{sc}}}{\sigma_{33\text{sc}0}}\left(\frac{\alpha}{\alpha_0}\right)^m \delta_0^* \tag{50}$$

This equation represents the midsurface in Fig. 8: the upper and lower bounds of the surface were determined considering the systematic scattering of ±20% recorded during

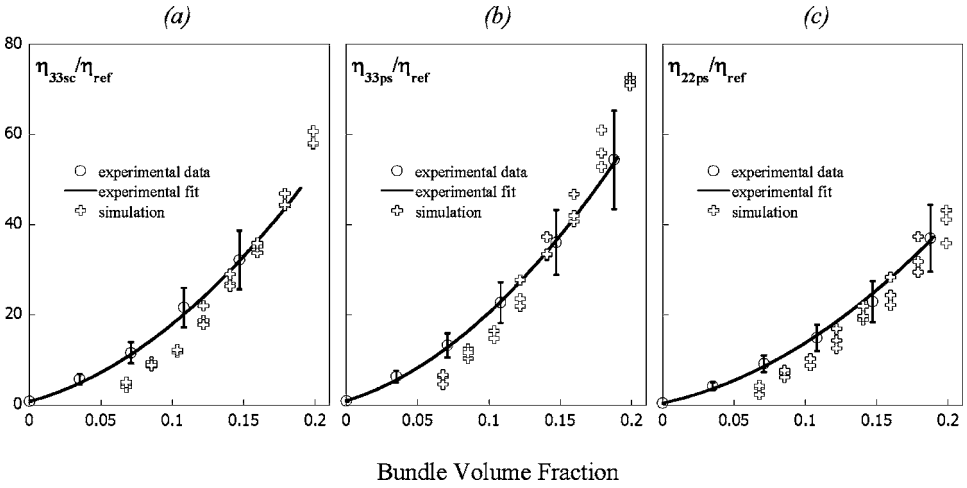

FIG. 9. Evolution of the normalized threshold viscosities with the volume fraction of bundles, comparison with experimental results obtained on an industrial SMC (Dumont *et al.*, 2003): (a) axial component in simple compression (33sc), (b) axial component in plane strain compression (33ps), (c) lateral component in plane strain compression (22ps).

the experiments (Dumont *et al.*, 2003). Servais *et al.* have tried to estimate the averaged sheared thickness α in highly concentrated glass bundles suspensions with thermoplastic matrix (Servais *et al.*, 1999a, 2002). They reported values ranging from 0.07 to 2.8 $\times 10^{-3}$ mm for bundles where cross section and length are not very different from ours. Using such estimates, the value of α was then fixed to 2×10^{-3} mm, leading to a value of δ^* of 3 (see Fig. 8). For the rest of the document, it was assumed that these values remained constant, whatever the bundles content, the deformation mode, and the imposed strain rate.

C. Comparison at the beginning of the flow

Given the values of constitutive parameters, a first set of numerical experiments was achieved and compared to experimental results obtained with the SMC at the beginning of the flow, i.e., at the threshold state

(1) The influence of the volume fraction of bundles on experimental and predicted results is given in Fig. 9. This figure shows the evolution of experimental and computed ratios η_{33sc}/η_{ref}, η_{33ps}/η_{ref} and η_{22ps}/η_{ref} with the volume fraction of bundles $f^{(f)}$. To obtain the computed threshold viscosities, simple and plane strain compressions were simulated with random microstructures at a compression rate $D_{33}^{(s)} = 1\ s^{-1}$: as it was proved that the suspension was a power-law fluid, these numerical experiments directly give the threshold viscosities [see for example the form of the power-law (45)]. Whatever the deformation mode, predictions are in rather good agreement with the experiments when the volume fraction of bundles is high ($f^{(f)} > 0.1$): this is the zone where the developed micro-macro approach holds. At lower bundle content ($f^{(f)} < 0.1$), the modeling of the suspension behavior could certainly be improved by adding to the overall stress tensor stress contributions accounted for in the theories of dilute or semidilute suspensions (Gibson and Toll. 1999; Souloumiac and Vincent, 1998).

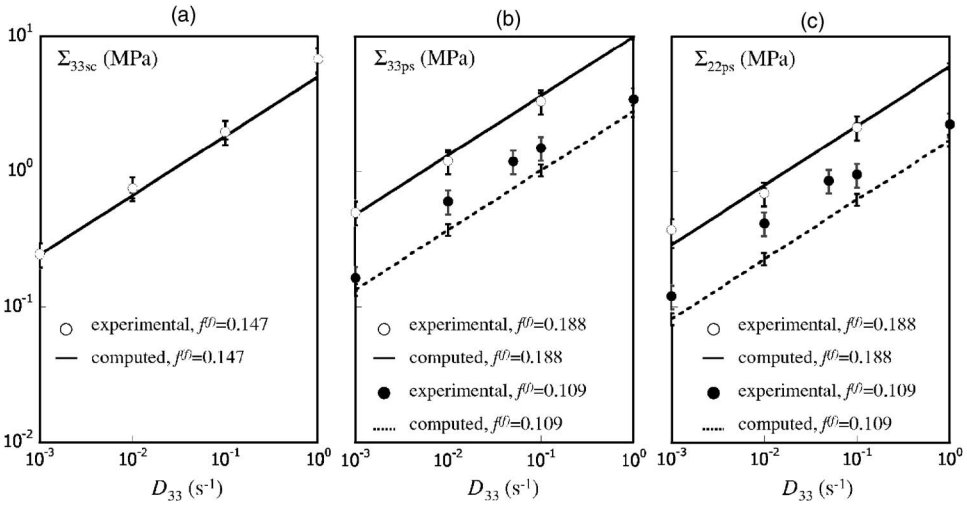

FIG. 10. Influence of the axial strain-rate D_{33} on the threshold stresses for a random suspension with various bundle content, comparison with experimental results of Dumont *et al.* (2003).

(2) Figure 10 clearly reveals the influence of the axial strain rate $D_{33}^{(s)}$ on the experimental and computed threshold stresses in simple or plane strain compressions. This figure also underlines the rather good correlation between experimental and predicted values.

(3) A scattering of the numerical results of about ±5% is systematically observed, as evident in Figs. 9 and 10. Such a discrepancy is ascribed to two combined reasons: (i) the random generation process used to build the bundles network and (ii) the use of only two very simple macroscopic quantities for the characterization of the generated networks, i.e., $f^{(f)}$ and $\widetilde{\boldsymbol{A}}$: it is well known that $f^{(f)}$ and $\widetilde{\boldsymbol{A}}$ only give rather coarse information and are not sufficient to fully characterize such microstructures (Batchelor, 1974).

D. Influence of the current orientation of the bundles

In a second stage, several bundle networks with the same fiber volume fraction ($f^{(f)}$ =0.188) and different orientations were generated and submitted to a plane strain compression test. The imposed strain rate $\widetilde{\boldsymbol{D}}^{(s)}(s^{-1})$ was then chosen such as

$$\widetilde{\boldsymbol{D}}^{(s)} = \boldsymbol{e}_1 \otimes \boldsymbol{e}_1. \tag{51}$$

Gaussian distributions of angles with a main direction along $\boldsymbol{e}_1$ or $\boldsymbol{e}_2$ and different standard deviations were used in order to obtain all the possible in-axis orientations for this kind of kinematics. This results in microstructures characterized by an almost diagonal orientation tensor $\widetilde{\boldsymbol{A}}$ with values of A_{11} ranging from 0, for perfectly aligned orientation along $\boldsymbol{e}_2$, to 1, for perfectly aligned orientation along e_1.

In Fig. 11(a), we analyze the influence of the current orientation state (equivalent to a snapshot in a time evolution problem), measured by A_{11}, on the computed components of $\boldsymbol{\sigma}^{(f)}$. In this figure, given a stress component, each point corresponds to a generated fiber net (about 85 networks with different orientations were used to obtain those data). As clear from this figure, the current bundle orientation noticeably influences the macro-

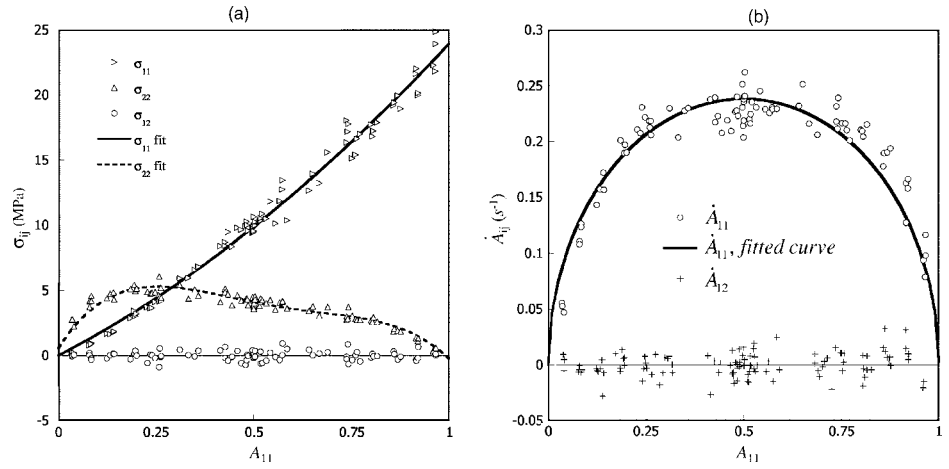

FIG. 11. Influence of the orientation intensity A_{11}, for fiber networks ($f^{(f)}=0.188$) undergoing a plane strain deformation along $\boldsymbol{e}_1$, ($D_{11}^{(s)}=-D_{33}^{(s)}=1s^{-1}$), and for $m=0.45$: (a) components of $\tilde{\boldsymbol{\sigma}}^{(f)}$, (b) components of $\dot{\tilde{\boldsymbol{A}}}$.

scopic mechanical behavior. The stress ratio $\sigma_{11}^{(f)}/\sigma_{22}^{(f)}$ is about 2.4 for random planar orientations ($A_{11}=0.5$), reaches values higher than 50 for A_{11} close to 1, and stresses tend to zero when A_{11} tends to zero. It is worth noting the scattering of the results and that the shear stress $\sigma_{12}^{(f)}$ is never exactly null, but always stays small compared to the main components $\sigma_{11}^{(f)}$ and $\sigma_{22}^{(f)}$: this is once again imputed to reasons given in Sec. V C 3.

The evolution of bundle orientation was analyzed in the same way through the evolution of $\dot{A}_{11}$ in terms of A_{11} and plotted in Fig. 11(b). Results here again underline the great effect of the current orientation state on the evolution of bundle orientation: as already observed in dilute and semidilute fiber suspensions, (i) the bundles tend to align in the direction of the flow ($\boldsymbol{e}_1$), (ii) the higher the deviation of A_{11} from 0.5, the lower the rate $\dot{A}_{11}$ (Advani and Tucker, 1990).

E. Comparison during the flow

Lastly, the predictions of the micro-macro model during simple and plane strain compressions were compared to experimental results obtained on the SMC.

(1) For the simple compression simulation, the initial isotropic orientation tensor $\tilde{\boldsymbol{A}}$ was first proved to remain constant during the deformation ($\dot{A}_{ij}\approx 0$), so that the computed viscous stress $\sigma_{11}^{(f)}$ ($=\sigma_{22}^{(f)}$ for isotropic microstructures) corresponds to that given at the beginning of the deformation, i.e., the threshold stress. Hence $\sigma_{11}^{(f)}$ was first estimated at an axial strain rate $D_{33}^{(s)}$ of -1 s^{-1}, and then modified for the experimental prescribed strain rate according to the property (29).

(2) For the plane strain compression along $\boldsymbol{e}_1$, it was first assumed that during the deformation of the sample, the orientation of the bundle network evolved from an initial isotropic state (i.e., perfectly random) to an oriented state such as the main orientation always stays in direction $\boldsymbol{e}_1$. The simulation was then achieved using the fitted curves presented in Fig. 11: for $\sigma_{11}(A_{11})$ we used a second-order polynomial fit, for $\sigma_{22}(A_{11})$ a fourth-order one, and for $\dot{A}_{11}(A_{11})$ we chose the expression $\dot{A}_{11,0}\sqrt{1-(2A_{11}-1)^2}$, with $\dot{A}_{11,0}=0.26$. Note that the fitting parameters have no physical meaning, they were just used here for the comparison with experimental data.

These curves allow one to determine at any time step t the viscous stresses $\sigma_{11}^{(f)}$ and $\sigma_{22}^{(f)}$ as well as the orientation rate $\dot{A}_{11}$, given the actual orientation A_{11} and the imposed strain rate $D_{33}^{(s)}=D_{11}^{(s)}=-1\ \mathrm{s}^{-1}$. The corresponding viscous stresses and orientation rate at the imposed experimental strain rate are then calculated thanks to properties (29) and (40), respectively. The time evolution of A_{11} was computed by an ordinary differential equations solver, using the fitted expression of $\dot{A}_{11}(A_{11})$.

Figure 7(a) then shows the evolution of the experimental and predicted total axial stress $\sigma_{33}^{(s)}$ during a simple compression test performed at $D_{33}^{(s)}=-0.01\ \mathrm{s}^{-1}$ ($f^{(f)}=0.188$). Figure 7(b) does the same for total stresses $\sigma_{22}^{(s)}$ and $\sigma_{33}^{(s)}$ and the orientation component A_{11} in the case of a plane strain compression test performed at $D_{33}^{(s)}=-0.01\ \mathrm{s}^{-1}$ ($f^{(f)}=0.188$). As visible from these figures, the present model rather well describes the experimental trends. In the particular case of the plane strain compression, it predicts an increase in stresses due to the increasing orientation of fiber in the direction of flow. This trend is well observed experimentally for the lateral stress $\sigma_{22\mathrm{ps}}$, however it is not really clear concerning the axial stress $\sigma_{33\mathrm{ps}}$. This point should be more precisely analyzed by additional experiments and would require to be checked for other bundle suspensions. Our calculations also provide explicitly the evolution of orientation during the flow which was not measured in Dumont *et al.* (2003). Further experimental investigations should be carried out to confirm these predictions of the model.

VI. DISCUSSION

To establish the micro-macro model, we have postulated *a priori* in Sec. III B that the equivalent macroscopic media of the considered bundles networks were usual Cauchy ones : this implies the local bundle-bundle interaction moments to be small $[\mathcal{O}(\epsilon)]$ with respect to the moments of bundle-bundle interaction forces. To check *a posteriori* the validity of such an assumption, three bundle networks with a bundle content of 0.188 and with three different orientations (random, rather and very oriented along $\boldsymbol{e}_1$) were submitted to four elementary mechanical loadings, i.e., plane strain compression along $\boldsymbol{e}_1$, plane strain compression along $\boldsymbol{e}_2$, pure shear in $\mathcal{P}$, and simple compression. From these macroscopic loadings, the ratio m_b^r was formed for each bundle b of the networks:

$$m_b^r=\frac{\Sigma_{b\in\mathcal{C}(b)}|M_k|}{\Sigma_{b\in\mathcal{C}(b)}\|s_b\boldsymbol{e}_b\times\boldsymbol{f}_k\|}. \tag{52}$$

This dimensionless ratio gauges the importance of local interaction moments active on a bar b with respect to the moment of forces acting on the same bar. Typically, the higher the averaged value of m_b^r in the REVs, the less valid the assumption of an equivalent macroscopic Cauchy medium. Figure 12 plots the evolution the fraction of bundles N_x/N matching a condition x on m_b^r for three networks with different bundle orientations in terms of this condition, expressed in % here ($m_b^r<x\%$). Such a representation gives an idea of the overall distribution of m_b^r in a given network. This figure, plotted for the four different simple flow kinematics, shows that for most fiber bundles and whatever the average orientation of the network, the value of m_b^r is lower than 5%. For the random and rather oriented cases [Figs. 12(a) and 12(b)], one even checks that more than 80% of the bundles match $m_b^r<2.5\%$, which is the order of the scale separation parameter ϵ. It is worth noticing that this trend is totally independent of macroscopic strain-rate. Those results are indeed in total agreement with the modeling assumptions adopted in this work (see Sec. III B) Figure 12(c) also shows that local moments become less and less negli-

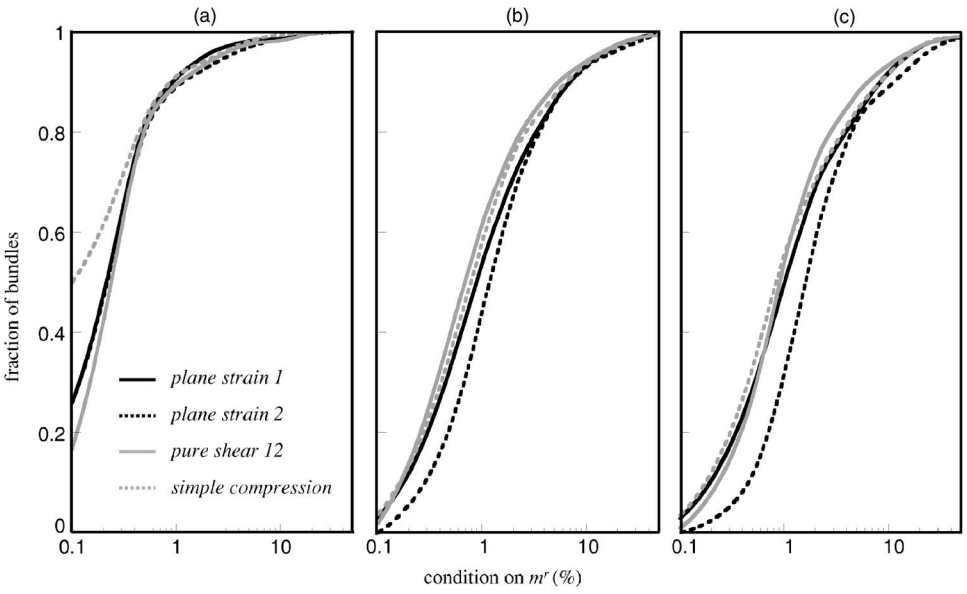

FIG. 12. Evolution of the fraction N_x/N, where N_x is the number of bundles such as $m_b^r < x$ and abscissa x is a condition expressed in %—different bundle networks with $f^{(f)}=0.188$ and $m=0.44$, submitted to four macroscopic strain rates: plane strain along $\boldsymbol{e}_1$, plane strain along $\boldsymbol{e}_2$, pure shear in direction 12, simple compression- (a) random orientation ($A_{11}=0.5$, $A_{12}=0$), (b) rather oriented ($A_{11}=0.82$, $A_{12}=-0.01$), (c) very oriented ($A_{11}=0.92$, $A_{12}=-0.009$).

gible as the orientation goes stronger. In this case, even if the major part of the histogram is below 5%, i.e., $\mathcal{O}(\epsilon)$, a greater number of moments ratios is above 5%. The effect of local moments on the macroscopic behavior could therefore become non-negligible for very oriented microstructures. Nevertheless, for industrial bundles suspensions such as GMT or SMC, these high orientation states are rarely encountered.

VII. CONCLUDING REMARKS

A numerical analysis based on the homogenization of discrete and periodic structures has been used to investigate the relationships between the microstructure and the macroscopic rheological properties of concentrated suspensions of fiber bundles having a mean planar orientation. The very high bundle content is such that bundles can be seen as forming a network of connected bundles that interact by direct mechanical contacts forces and moments during the deformation of the suspension. Nonlinear power-law type viscous bundle-bundle interaction mechanisms were taken into account in the modelling, and a rigid motion assumption of the bundles was postulated in the mean plane of the suspension. In order to study the rheology of suspensions close to industrial short fiber composites such as GMT or SMC, a generation procedure of REVs has been proposed to build idealized concentrated suspensions having different bundle orientations and volume fractions. This enabled us, by means of "numerical rheometry experiments" performed for various flow kinematics, to highlight and quantify the strong influence of microstructural parameters on the mechanical behavior of the suspensions.

A first interesting result was obtained concerning the influence of the macroscopic strain rate on the macroscopic stress tensor. It was shown that if the microscopic bundle-bundle interactions are of power-law viscous type, the whole suspension has a power-law

fluid behavior, with a power-law index identical at the microscopic and macroscopic levels. It was also proved that the rate of the second-order orientation tensor is an homogeneous function of a degree one with respect to the macroscopic velocity gradient tensor, whatever the nature of the interaction viscous bonds (linear or power-law). Note that these two fundamental properties are proved theoretically, independently of the REVs generation procedure. Furthermore, thanks to the analysis of the general form of the constitutive equations of the equivalent continuum, the stress levels were shown to be quadratic functions of the volume fraction of bundles. This is directly induced by the method used to detect bundle-bundle contacts in the generated REVs, a method that follows the statistical tube model framework (Toll, 1993). At last, it was also shown that for the suspension under consideration, local interaction moments can be considered as small quantities with respect to the moments of interaction forces, so that the suspensions can be reasonably seen as usual Cauchy media at the macroscopic level.

It must be pointed out that the proposed model only requires a small set of constitutive parameters, all of them being directly linked to the physics and the geometry at the bundle scale. A simple methodology has been given for their estimation. The predictions of this model of idealized concentrated suspensions were then compared with results obtained with industrial SMC materials. Despite the very simple assumptions postulated at the bundle scale, results show a fairly good agreement concerning the predicted threshold viscosities or stresses that were measured in simple compression or plane strain compression tests, in the interesting domain of volume fraction. The strong influence of the current bundle orientation on the stress as well as on the orientation rate tensor was also highlighted in the example of a plane strain compression. At last, comparison with experimental results show that the present model can also predict the evolution of stresses during the flow.

However, the very simple geometrical, kinematical, and mechanical assumptions stated at the bundle scale should be further validated or improved. The possible improvement could for example be achieved performing rheometry experiments on a well-chosen highly concentrated suspension that would allow the analysis of the motion of the bundles during the flow. This was unfortunately impossible with the opaque SMC matrix. The analysis of such a model material could give answers to the following questions : what is the geometry, the microstructure, and the rheology of the entrapped medium? (How) do the contact zones evolve? (How) do the bundles flatten? (How) do the bundles bend in the plane of the sheet?

Moreover, further systematic numerical rheometry experiments are needed to explore more precisely in a wider range of flow kinematics and microstructural parameters: (i) the macroscopic stress tensor, (ii) the evolution of the orientation of the bundles, (iii) the difference between the linear and power-law behaviors, (iv) the relation between bundle orientation and mechanical anisotropy, (v) the impact of generation strategy. This would constitute a precious database that could be compared with both existing linear and nonlinear macroscopic stress models developed for semidilute and concentrated fiber/bundle suspensions, and to existing models of fiber orientation evolution.

ACKNOWLEDGMENTS

The authors wish to thank the Région Rhône-Alpes and the industrial partners Schneider Electric, Renault, Groupe Mecelec-Inoplast and Renault Trucks, for their support.

References

Advani, S., *Flow and Rheology in Polymer Composites Manufacturing*, Composite Materials Series Vol. 10 (Elsevier, New York, 1994).

Advani, S. G., and C. L. Tucker, "The use of tensors to describe and predict fiber orientation in short fiber composites," J. Rheol. **31**, 751–784 (1987).

Advani, S. G., and C. L. Tucker, "Closure approximations for the three-dimensional structure tensors," J. Rheol. **34**, 367–386 (1990).

Auriault, J.-L., "Heterogeneous medium. Is an equivalent macroscopic description possible?," Int. J. Eng. Sci. **29**, 785–795 (1991).

Ausias, G., J. F. Agassant, M. Vincent, P. G. Lafleur, P. A. Lavoie, and P. J. Carreau, "Rheology of short glass fiber reinforced polypropylene," J. Rheol. **36**, 525-542 (1992).

Batchelor, G., "The stress system in a suspension of force-free particles," J. Fluid Mech. **41**, 545–570 (1970a).

Batchelor, G. K., "Slender-body theory for particles of arbitrary cross-section in Stokes flow," J. Fluid Mech. **44**, 419–440 (1970b).

Batchelor, G. K., "The stress generated in a non-dilute suspension of elongated particles by pure straining motion," J. Fluid Mech. **46**, 813–829 (1971).

Batchelor, G. K., "Transport properties of two-phase materials with random structure", Annu. Rev. Fluid Mech. **6**, 227–255 (1974).

Bensoussan, A., J.-L. Lions, and G. Papanicolaou, *Asymptotic Analysis for Periodic Structures* (North Holland, Amsterdam, 1978).

Berglund, L. A., and M. L. Ericson, *Polypropylene: Structure, Blends and Composites*, edited by J. Karger-Kocis (Chapman and Hall, London, 1995), Chap. 5.

Boutin, C., and S. Hans, "Homogenisation of periodic discrete medium: Application to dynamics framed structures," Comput. Geotech. **30**, 303–320 (2003).

Bretherton, F. P., "The motion of rigid particles in a shear flow at low Reynolds number," J. Fluid Mech. **14**, 284–304 (1962).

Chung, D. H., and T. H. Kwon, "Fiber orientation in the processing of polymer composites," Korea-Aust. Rheol. J. **14**, 175–188 (2002).

Cintra, J. S., and C. L. Tucker III, "Orthotropic closure approximations for flow-induced fiber orientation," J. Rheol. **39**, 1095–1122 (1995).

Cosserat, E., and F. Cosserat, *Théorie Des Corps Déformables*, Herman et fils edition (Paris, 1909).

Dinh, M. S., and R. C. Armstrong, "A rheological equation of state for semiconcentrated fiber suspensions," J. Rheol. **28**, 207–227 (1984).

Doi, M., and S. F. Edwards, "Dynamics of rod-like macromolecules in concentrated solution," J. Chem. Soc., Faraday Trans. 2 **74**, 560–570 (1978).

Dumont, P., L. Orgéas, S. Le Corre, and D. Favier, "Anisotropic viscous behaviour of sheet molding compounds (SMC) during compression molding," Int. J. Plast. **19**, 625–646 (2003).

Dupret, F., and V. Verleye, *Modelling the Flow of Fiber Suspensions in Narrow Gaps* (Elsevier, Amsterdam, 1999), pp. 1347–1398.

Ericsson, K. A., S. Toll, and J.-A. E. Månson, "Sliding plate rheometry of planar oriented concentrated fiber suspension," Rheol. Acta **36**, 397–405 (1997).

Fan, X., N. Phan-Thien, and R. Zheng, "A direct simulation of fibre suspensions," J. Non-Newtonian Fluid Mech. **74**, 113–135 (1998).

Folgar, F., C. Tucker, and C. Lee, "Simulation of compression molding for fiber-reinforced thermosetting polymers", J. Eng. Ind. **106**, 114–125 (1984).

Galdi, G. P., and B. D. Reddy, "Well-posedness of the problem of fiber suspension flows," J. Non-Newtonian Fluid Mech. **83**, 205–230 (1999).

Germain, P., "The method of virtual power in continuum mechanics. II : Microstructure," SIAM J. Appl. Math. **25**, 556–575 (1973).

Gibson, A., and S. Toll, "Mechanics of the squeeze flow of planar fibre suspensions", J. Non-Newtonian Fluid Mech. **82**, 1–24 (1999).

Goddard, J. D., "Tensile stress contribution of flow-oriented slender particles in non-Newtonian fluids", J. Non-Newtonian Fluid Mech. **1**, 1–17 (1976).

Greene, J., and J. Wilkes, "Numerical analysis of injection molding of glass fiber reinforced thermoplastics. 2. Fiber orientation," Polym. Eng. Sci. **37**, 1019–1035 (1997).

Hamada, H., G. O. Shonaike, S. Yamaguchi, T. Sato, Z. Maekawa, and M. Koshimoto, "Flow behavior of stampable sheet with a rib part," Polym. Compos. **15**, 393–400 (1994).

Hand, G. L., "A theory of anisotropic fluids," J. Fluid Mech. **13**, 33–46 (1962).

Hinch, E. J., and L. G. Leal, "Constitutive equations in suspension mechanics. 1. General formulation," J. Fluid Mech. **71**, 481–495 (1975).

Hinch, E., and L. Leal, "Constitutive equations in suspension mechanics. 2. Approximate forms for a suspension of rigid particles affected by Brownian rotations," J. Fluid Mech. **76**, 187–208 (1976).

Jeffery, G. B., "The motion of ellipsoidal particles immersed in a viscous fluid," Proc. R. Soc. London, Ser. A **102**, 161–179 (1922).

Joung, C. G., N. Phan-Thien, and X. J. Fan, "Direct simulation of flexible fibers," J. Non-Newtonian Fluid Mech. **99**, 1–36 (2001).

Joung, C. G., N. Phan-Thien, and X. J. Fan, "Viscosity of curved fibers in suspension," J. Non-Newtonian Fluid Mech. **102**, 1–17 (2002).

Koch, D. L., "A model for orientational diffusion in fiber suspensions," Phys. Fluids **7**, 2086–2088 (1995).

Koch, D. L., and E. S. G. Shaqfeh, "The average rotation rate of a fiber in the linear flow of a semidilute suspension," Phys. Fluids A **2**, 2093–2102 (1990).

Le Corre, S., D. Caillerie, L. Orgéas, and D. Favier, "Behavior of a net of fibers linked by viscous Interactions: Theory and mechanical properties," J. Mech. Phys. Solids **52**, 395–421 (2004).

Le Corre, S., L. Orgéas, D. Favier, A. Tourabi, A. Maazouz, and C. Venet, "Shear and compression behaviour of sheet molding compounds," Compos. Sci. Technol. **62**, 571–577 (2002).

Lipscomb, G. G., M. M. Denn, D. U. Hur, and D. V. Boger, "The flow of fiber suspensions in complex geometries", J. Non-Newtonian Fluid Mech. **26**, 297–325 (1988).

Mackaplow, M. B., and E. S. G. Shaqfeh, "A numerical study of the rheological properties of suspensions of rigid, non-brownian fibres," J. Fluid Mech. **329**, 155–186 (1996).

Moreau, G., and D. Caillerie, *Proceedings of Civil Comp' 95* (Civil Comp, Edinburgh, UK, 1995).

Moreau, G., and D. Caillerie, "Continuum modeling of lattice structures in large displacement-applications to buckling analysis," Comput. Struct. **68**, 181–189 (1998).

Munganga, J. M. W., B. D. Reddy, and K. J. Diatezua, "Aspects of the thermodynamic stability of fibre suspension flows," J. Non-Newtonian Fluid Mech. **92**, 135–150 (2000).

Osswald, T., and S.-C. Tseng, *Flow and Rheology in Polymer Composites Manufacturing* (Elsevier, Amsterdam), 1994, Chap. 10.

Petrich, M. P., and D. L. Koch, "Interactions between contacting fibers," Phys. Fluids **10**, 2111–2113 (1998).

Petrich, M. P., D. L. Koch, and C. Cohen, "An experimental determination of the stress-microstructure relationship in semi-concentrated fiber suspensions," J. Non-Newtonian Fluid Mech. **95**, 101–133 (2000).

Phan-Thien, N., X. J. Fan, R. I. Tanner, and R. Zheng, "Folgar-Tucker constant for a fibre suspension in a Newtonian fluid," J. Non-Newtonian Fluid Mech. **103**, 251–260 (2002).

Phan-Thien, N., and A. L. Graham, "A new constitutive model for fibre suspensions: Flow past a sphere," Rheol. Acta **30**, 44–57 (1991).

Pradel, F., and K. Sab, "Cosserat modelling of periodic lattice structure," C. R. Acad. Sci., Ser. IIb: Mec., Phys., Chim., Astron. **326**, 699–704 (1998).

Rahnama, M., D. L. Koch, and C. Cohen, "Observations of fiber orientation in suspensions subjected to planar extensional flows," Phys. Fluids **7**, 1811–1817 (1995).

Ranganathan, S., and S. G. Advani, "Fiber-fiber interactions in homogeneous flows of non-dilute suspensions," J. Rheol. **35**, 1499–1522 (1991).

Sanchez-Palencia, E., *Non-Homogeneous Media and Vibration Theory*, Lecture Notes in Physics (Springer, Berlin, 1980).

Servais, C., A. Luciani, and J.-A. E. Månson, "Fiber-fiber interaction in concentrated suspensions: Dispersed fiber bundles," J. Rheol. **43**, 1005–1018 (1999a).

Servais, C., A. Luciani, and J.-A. E. Månson, "Squeeze flow of concentrated long fibre suspensions: Experiments and model," J. Non-Newtonian Fluid Mech. **104**, 165–184 (2002).

Servais, C., J.-A. E. Månson, and S. Toll, "Fiber-fiber interaction in concentrated suspensions: Disperse fibers," J. Rheol. **43**, 991–1004 (1999b).

Shaqfeh, E. S. G., and D. Koch, "Orientational dispersion of fibers in extensional flows," Phys. Fluids A **2**, 1077–1093 (1990).

Souloumiac, B., and M. Vincent, "Steady shear viscosity of short fibre suspensions in thermoplastics," Rheol. Acta **37**, 289–298 (1998).

Sundararajakumar, R. R., and D. L. Koch, "Structure and properties of sheared fiber suspensions with mechanical contacts," J. Non-Newtonian Fluid Mech. **73**, 205–239 (1997).

Switzer, L. H., and D. J. Klingenberg, "Rheology of sheared flexible fiber suspensions via fiber-level simulations," J. Rheol. **47**, 759–778 (2003).

Thomasson, J. L., and M. A. Vlug, "Influence of fibre length and concentration on the properties of glass fibre-reinforced polypropylene. 1. Tensile and flexural modulus," Composites, Part A **27A**, 477–484 (1996).

Toll, S., "Note: On the tube model for fiber suspensions," J. Rheol. **37**, 123–125 (1993).

Toll, S., and J.-A. E. Månson, "Dynamics of a planar concentrated suspension with non-hydrodynamic interaction," J. Rheol. **38**, 985–997 (1994).

Tollenaere, H., and D. Caillerie, "Continuous modeling of lattice structures by homogenization," Adv. Eng. Software **29**, 699–705 (1998).

Truesdell, C., and W. Noll, *The Non-linear Field Theories of Mechanics*, 2nd ed. (Springer, New York, 1965), Vol. 3, chap. 3, corrected 1992.

Yamane, Y., Y. Kaneda, and M. Doi, "The effect of interaction of rodlike particles in semi-dilute suspensions under shear flow," J. Phys. Soc. Jpn. **64**, 3265–3274 (1995).